JGR Atmospheres

RESEARCH ARTICLE
10.1029/2020JD033829

Special Section:
Stratospheric aerosol during the post Pinatubo era: processes, interactions, and impact

How Does a Pinatubo-Size Volcanic Cloud Reach the Middle Stratosphere?

Georgiy Stenchikov[1], Alexander Ukhov[1], Sergey Osipov[1,2], Ravan Ahmadov[3,4], Georg Grell[4], Karen Cady-Pereira[5], Eli Mlawer[5], and Michael Iacono[5]

[1]King Abdullah University of Science and Technology, Thuwal, Saudi Arabia, [2]Max Planck Institute for Chemistry, Mainz, Germany, [3]CIRES, University of Colorado, Boulder, CO, USA, [4]NOAA Earth Systems Research Laboratory, Boulder, CO, USA, [5]Atmospheric and Environmental Research, Lexington, MA, USA

Abstract Volcanic explosions are the most critical replenishing mechanism of the stratospheric aerosol Junge layer. A fresh volcanic cloud comprises mostly sulfur-bearing gases, volcanic ash, and water vapor. It is commonly assumed that only sulfate aerosols remain in an aged volcanic cloud. Accurate simulation of the initial evolution of multicomponent fresh volcanic clouds is largely missing due to insufficient spatial resolution and a lack of relevant physics in global climate models. However, this initial stage is essential, as the vertical structure, composition, and altitude of a freshly developed volcanic cloud affect its long-term evolution. To fill this gap, we modified a regional WRF-Chem model to study the dispersion of a Pinatubo-size volcanic cloud in the equatorial belt with a 25 km grid spacing explicitly accounting for the SO_2, ash, sulfate, water vapor, and hydrometeors radiative effects. The model best reproduces the observed evolution of the Pinatubo optical depth when eruptive products are injected above the cold tropical tropopause at 17 km. During the first week, the volcanic cloud in our simulations rises 1 km/day. Ash is primarily responsible for the heating and lofting of the volcanic products. Radiative heating of SO_2 is weaker than that of ash and sulfate but is sufficient to position the core of the SO_2 layer 1–2 km above the sulfate layer. Utilizing a more realistic description of the volcanic cloud's initial stage potentially improves overall volcanic cloud predictability. It might also be essential to designing geoengineering technologies based on the injection of aerosol precursors in the lower stratosphere.

Key Points:

- The model better reproduces the observed evolution of the Pinatubo optical depth when eruptive products are injected at 17 km
- The short-lived ash is primarily responsible for the heating of the volcanic cloud
- Radiative heating of SO_2 is weaker than that of ash and sulfate aerosols but still is significant to position the core of the SO_2 cloud 1–2 km above the sulfate layer

Correspondence to:
G. Stenchikov,
georgiy.stenchikov@kaust.edu.sa

Citation:
Stenchikov, G., Ukhov, A., Osipov, S., Ahmadov, R., Grell, G., Cady-Pereira, K., et al. (2021). How does a Pinatubo-size volcanic cloud reach the middle stratosphere? *Journal of Geophysical Research: Atmospheres*, *126*, e2020JD033829. https://doi.org/10.1029/2020JD033829

Received 2 SEP 2020
Accepted 5 MAY 2021

Author Contributions:
Conceptualization: Georgiy Stenchikov
Data curation: Alexander Ukhov
Formal analysis: Georgiy Stenchikov, Alexander Ukhov
Funding acquisition: Georgiy Stenchikov
Investigation: Georgiy Stenchikov, Alexander Ukhov, Sergey Osipov
Methodology: Georgiy Stenchikov, Alexander Ukhov, Sergey Osipov,

1. Introduction

Stratospheric aerosols significantly affect the Earth's energy balance and atmospheric and ocean circulation (Pollack et al., 1976; Ramaswamy et al., 2019; Robock, 2000; Sigl et al., 2015; Stenchikov, 2016; Timmreck, 2012). Their abundance is maintained by explosive volcanism, meteoric materials, and cross-tropopause transport of sulfur-containing compounds (Bardeen et al., 2008; Brock et al., 1995; Brühl et al., 2012; Crutzen, 1976; Fueglistaler et al., 2009; Gómez Martín et al., 2017; Kremser et al., 2016; Sheng et al., 2015). The balance between vertical ascent and gravitational settling stabilizes the long-lived stratospheric aerosols at the level of neutral buoyancy within the Junge layer (Junge & Manson, 1961). Integrated over time volcanic contributions to the Junge layer prevail over those of anthropogenic emissions and meteoric processes (Bardeen et al., 2008; Carn et al., 2016; Gómez Martín et al., 2017; Kremser et al., 2016; Neely III et al., 2013; Vernier et al., 2011).

Volcanic explosions inject volcanic ash, sulfur-bearing gases (mostly SO_2), water vapor, CO_2, halogens, N_2, and other species into the lower stratosphere (Textor et al., 2004). Ash, SO_2, and later generated sulfate aerosols are the most important because of their radiative effect. The evolution of a volcanic cloud is affected by fine-scale dynamic processes initiated by cloud heating (Aquila et al., 2012; Gerstell et al., 1995; Kinne et al., 1992; Niemeier et al., 2009; Oman et al., 2006; Young et al., 1994).

In climate model simulations, it is often assumed that volcanic debris from strong Plinian volcanic eruptions (with volcanic explosivity index VEI ≥ 6) is delivered into the stratosphere by eruptive jet (Aubry et al., 2016; Mills et al., 2016; Schmidt et al., 2018) and soon after an eruption reaches the layer of neutral buoyancy in the middle stratosphere, where aged aerosol-cloud resides. But volcanic debris could also be delivered into the lower stratosphere by co-ignimbrite convection. In this case, volcanic material is released just above the tropopause. The low injection height of 17–18 km was suggested in the recent modeling and observation studies of the 1991 Pinatubo eruption (Aquila et al., 2012; Brühl et al., 2018; Fisher et al., 2019).

Ravan Ahmadov, Georg Grell, Karen Cady-Pereira, Eli Mlawer, Michael Iacono
Project Administration: Georgiy Stenchikov
Resources: Georgiy Stenchikov
Software: Alexander Ukhov, Sergey Osipov, Ravan Ahmadov, Georg Grell, Karen Cady-Pereira, Eli Mlawer, Michael Iacono
Supervision: Georgiy Stenchikov
Validation: Georgiy Stenchikov, Alexander Ukhov
Visualization: Alexander Ukhov, Sergey Osipov
Writing – original draft: Georgiy Stenchikov
Writing – review & editing: Georgiy Stenchikov

If volcanic materials are released above the tropopause, radiative heating of volcanic cloud is then essential to raise it to the middle stratosphere. Lofting of volcanic debris is a complex process that depends on the concentration of optically active eruptive products, aerosol microphysics, and radiative properties of volcanic materials. As we show, for a Pinatubo-size cloud, the lifting velocity soon after injection is much higher than that in large-scale equatorial stratospheric uplift (Neely III et al., 2013; Rosenlof, 1995; Vernier et al., 2011). Understanding the evolution of fresh SO_2 or aerosol clouds in the lower stratosphere could also improve the Solar Radiation Management technology suggested for geoengineering of Earth's climate (Caldeira et al., 2013; Rasch et al., 2008; Shepherd, 2009).

The volcanic injection itself lasts typically from a few hours to a day. The height of an injection can be estimated using one-dimensional (1-D) models of turbulent buoyant plumes (Costa et al., 2016; Morton et al., 1956; Woods, 2010). However, the processes at the initial stage of a volcanic injection are described more realistically by three-dimensional (3-D) cloud-resolving models explicitly simulating plume dynamics and aerosol microphysics in eruptive column (Herzog et al., 1998; Suzuki et al., 2016; Textor et al., 2003). But these models are computationally expensive and only allow the study of volcanic plume dispersion for a relatively short time within 100–150 km from the emission site.

Here, we focus on the 1991 Pinatubo eruption in the Philippines that was the largest volcanic explosion in the 20th century, emitting about 14–20 Mt of SO_2 in the tropical lower stratosphere (Bluth et al., 1992, 1993; Fisher et al., 2019; Guo, Bluth, et al., 2004; Guo, Rose, et al., 2004; Holasek et al., 1996; McCormick et al., 1995). This eruption has become a case-study of volcanic aerosols' strong climate impact (Hansen et al., 1992; Kinne et al., 1992; Kirchner et al., 1999; Stenchikov et al., 1998).

Even though the 1991 Mt. Pinatubo eruption is the best observed strong explosive event, the information about the initial stage of the eruption is limited. Stratospheric Aerosol and Gas Experiment (SAGE) missed the initial phase of the eruption. The airborne lidar observations conducted on July 7–14, 1991, in the equatorial latitudes of 4.5°S–14.5°N detected reflective aerosol layers at altitudes 18–23 km (Winker & Osborn, 1992). Self et al. (1996) and Guo, Bluth, et al. (2004) found the initial SO_2 injection height to be in the range of 18–25 km.

It is usually assumed that soon after injection there is little sulfate in a volcanic cloud, as SO_2 photochemical oxidation takes weeks (Bluth et al., 1992; Read et al., 1993). However, Guo, Rose, et al. (2004) suggested that the fresh Pinatubo cloud initially might contain 4 Mt of sulfate of non-photochemical origin. Dhomse et al. (2014) in their Pinatubo simulations emitted 3% of SO_2 as sulfuric acid particles (equivalent to 0.75 Mt of dry SO_4). LeGrande et al. (2016) found that accounting for volcanic water in a fresh cloud accelerates SO_2 oxidation in the early stage. But Osipov et al. (2020) pointed out that in a fresh cloud ultra violet (UV) absorption by SO_2, ash, and sulfate aerosols inhibits ozone photolysis and SO_2 oxidation. Recently, Zhu et al. (2020) found that heterogeneous reactions of SO_2 on ash can rapidly convert some SO_2 to sulfate.

When developed, aerosol particles experience coagulation and condensation growth, and are removed from the stratosphere by atmospheric transport and gravitational settling (Hamill et al., 1997; Pueschel, 1996; Turco et al., 1982). Thus, in the long-term, aerosol microphysics control both the volcanic cloud optical characteristics and lifetime. For example, in massive volcanic injections, due to a higher concentration of SO_2 and H_2SO_4, sulfate aerosols particles grow rapidly. Their effective radius could exceed 1 μm so that gravitational settling quickly removes them. This mechanism effectively restricts climate impact of large eruptions (Osipov et al., 2020; Pinto et al., 1989; Timmreck et al., 2010).

Volcanic ash particles are larger than sulfate aerosol ones exceeding 2–3 μm in diameter, and their settling velocities are greater than 1 km/day (Guo, Rose, et al., 2004; Kasten, 1968; Niemeier et al., 2009; Wiesner et al., 2004). Although ash immediately after eruption develops a measurable radiative effect, its mass diminishes rapidly suggesting that ash itself could not produce a long-term climate impact. The finest ash particles, though, may remain in the stratosphere for a few months after an eruption but their radiative effect is negligible (Guo, Rose, et al., 2004; Niemeier et al., 2009). Still, ash at the initial stage, due to its high absorption in shortwave (SW) and longwave (LW), could cause strong radiative heating within the volcanic cloud and affect its dynamics (Niemeier et al., 2009).

Sulfur-rich volcanic eruptions that are also very energetic (VEI ≥ 6) could increase the sulfur content in the stratosphere by up to two orders of magnitude. Conversely, because the stratosphere contains so much water (about 1 Gt) it is difficult for volcanic eruptions to greatly perturb stratospheric water globally. The mass of volcanic water injections is at least 10 times smaller than the total accumulated stratospheric water. A significant immediate increase in stratospheric water after volcanic eruptions was never observed (Dessler et al., 2014; Fueglistaler, 2012; Fueglistaler et al., 2009). It was even suggested that oxidation of giant volcanic SO_2 injections could consume a significant amount of stratospheric water depleting its stratospheric content (Bekki, 1995; Pinto et al., 1989). However, the enhanced abundance of absorbing aerosols near the tropopause layer can heat the tropopause, increasing influx of tropospheric water vapor into the stratosphere that overwhelms the chemical depletion of stratospheric water (Considine et al., 2001; Fueglistaler et al., 2013; Joshi & Shine, 2003; Osipov et al., 2020; Randel et al., 2004; Robock et al., 2009). Injected "volcanic" stratospheric water facilitates the generation of OH radicals that control SO_2 oxidation. Thus, it is important to correctly calculate the amount of stratospheric water and account for OH's interactive generation in the stratosphere (Clyne et al., 2020).

The importance of differential heating of volcanic debris for dynamics of a volcanic cloud was already recognized at the time of El Chichon and Pinatubo eruptions (Gerstell et al., 1995; Kinne et al., 1992; Lary et al., 1994; Zhong et al., 1996). Gerstell et al. (1995) estimated heating rates caused by SO_2, sulfate aerosols, and silicate ash following the El Chichon eruption in 1982. They found that SO_2 and sulfate produce heating rates of the order of 1 K/day, while volcanic ash heating rates could be one order of magnitude larger. This radiative heating is balanced by vertical uplift. The authors mention that in spite of their limited spatial and temporal extent, SO_2 absorption can have a considerable effect on the height of a volcanic cloud. Kinne et al. (1992) argued that the induced vertical motion leads to the upward shift of the equatorial ozone profile in about 5 months after the 1991 Pinatubo eruption. This tends to compensate for the volcanic aerosol heating effect. However, none of the early studies account for the dynamic processes comprehensively.

Short-term volcanic cloud forecasts for aviation purposes were conducted using Volcanic Ash Transport and Dispersion, and Regional Mesoscale models, but they do not account for the radiative effects of aerosols (Fero et al., 2009; Folch et al., 2016; H. Vogel et al., 2014). 2-D climate models shed light on many fundamental aspects of long-term evolution of volcanic clouds (Bekki & Pyle, 1994; Tie et al., 1994; Weisenstein et al., 1997; Zhao et al., 1995), but are unable to resolve the initial 3-D fresh volcanic cloud development. The global chemistry-climate models are capable of simulating the long-term large-scale evolution of volcanic clouds. They calculate their dispersion by the Brewer-Dobson (BD) circulation (Holton et al., 1995) that is affected by the phase of the Quasi-Biennial-Oscillation (QBO) (Trepte & Hitchman, 1992), as well as perturbations coming from the troposphere (Jones et al., 2016). They treat volcanic aerosols with different levels of complexity, sometimes assuming that the SO_2 cloud is zonally uniform at a time of eruption, do not account for the radiative effect of SO_2, and do not emit ash and water vapor along with SO_2. Global models cannot adequately calculate the initial dispersion of a volcanic cloud, due to their coarse spatial resolution. Aerosol microphysics is extremely important for evolution of volcanic cloud, but remains poorly constrained (Clyne et al., 2020).

Young et al. (1994) and Timmreck et al. (1999) were the first to simulate volcanic sulfate clouds interactively in a 3-D General Circulation Model (GCM). Oman et al. (2006) and (Aquila et al., 2012) accounted for radiative feedback of a sulfate cloud. Niemeier et al. (2009) injected volcanic ash along with SO_2. Brühl et al. (2015, 2018), Mills et al. (2016), and Schmidt et al. (2018) implemented high-quality SO_2 emission observations to calculate the volcanic radiative forcing. LeGrande et al. (2016) accounted for the effect of volcanic water on new particle formation. Timmreck et al. (2010), Brühl et al. (2012), Dhomse et al. (2014), and Sekiya et al. (2016) approximate aerosol size distributions using a few lognormal modes with prescribed width and calculate the evolution of their modal radii. English et al. (2013) and Mills et al. (2016) use the most accurate and time-consuming sectional approximation of aerosol size distribution.

Despite the impressive improvements in the description of the physical processes in volcanic clouds, the uncertainties of the state-of-the-art model estimates remain relatively high (Clyne et al., 2020; Timmreck et al., 2018). The poor description of the initial stage of volcanic cloud dispersion in the coarse-resolution global models may be partially to blame for this. The important parameters of the fresh volcanic cloud that comprise injected masses of ash and SO_2, size distribution of ash, and height of injection of volcanic debris

are uncertain (Fisher et al., 2019; Gouhier et al., 2019; Mastin et al., 2009). The recent reprocessing of satellite observations from multiple sensors (Fisher et al., 2019) suggests that the injection height of the 1991 Pinatubo eruption was at 18 km, just above the tropical tropopause. This is consistent with the hypothesis that a significant portion of volcanic debris was delivered to the lower stratosphere by co-ignimbrite convection.

The pollutants (anthropogenic or from small volcanic eruptions) that penetrated the equatorial lower stratosphere are lifted within the ascending branch of the BD circulation. But this uplift is relatively slow, with an effective speed of 10–20 m/day (Rosenlof, 1995), so it takes 1–2 years for tracers from the lower stratosphere to reach the middle stratosphere (Neely III et al., 2013; Vernier et al., 2011). However, after a big explosion, like the 1991 Pinatubo event, the volcanic materials initially are concentrated in a relatively small volume, so that radiative heating of volcanic debris generates significant positive buoyancy, which could cause their quick rising. At the same time, ash and sulfate particles are settling gravitationally; ash much faster than sulfate aerosols (ash—1 km/day, sulfate—100 m/day). SO_2, SO_4, ash, and water vapor, affect radiative heating and lifting of a volcanic cloud. Osipov et al. (2020) have exploited the ability of GISS Model-E to calculate the SO_2 greenhouse effect, but SO_2 solar heating for the Earth's atmosphere, to the best of our knowledge, has been implemented previously only in a 2-D dynamical model (Gerstell et al., 1995).

To calculate the initial evolution of the Pinatubo volcanic cloud with high spatial resolution accounting for the above physical complexity, we use the open-source comprehensive community regional Weather Research Forecasting Model coupled with the aerosol-chemistry module, WRF-Chem v3.7.1 (Grell et al., 2005; Powers et al., 2017; Skamarock et al., 2005). We modify WRF-Chem to calculate the sulfur cycle in the stratosphere accounting for the radiative effect of SO_2, volcanic ash, sulfate aerosols, water vapor, and hydrometeors. So that here using WRF-Chem added "stratospheric" capabilities, we aim at calculating the initial stage of volcanic cloud development and testing the comparative importance of physical effects that govern a volcanic cloud dispersion. We conduct fine-resolution simulations of the 1991 Pinatubo eruption targeting the following science questions:

- How does the fresh volcanic cloud with simultaneously injected SO_2, ash, water vapor, and gradually accumulating sulfate aerosols develop during the first months after the injection?
- How does the radiative heating of eruptive products, water vapor injections, and initial detrainment height, affect volcanic cloud transport and dispersion?
- What is the most plausible Pinatubo initial injection height consistent with the observed altitude of the volcanic cloud, masses of injected materials, and their observed optical depth?

2. Model Setup

In this study, we employ WRF-Chem v3.7.1 (Grell et al., 2005; Powers et al., 2017; Skamarock et al., 2005), which is widely used to calculate processes in the troposphere (Kalenderski & Stenchikov, 2016; Ukhov et al., 2021; Ukhov, Mostamandi, da Silva, et al., 2020; Ukhov, Mostamandi, Krotkov, et al., 2020). In all the simulations discussed below, we configure the meteorological component of WRF-Chem with the Unified Noah land surface model and use the Revised MM5 Monin-Obukhov scheme to represent land surface processes and surface layer physics. The Yonsei University scheme is chosen for planetary boundary layer parameterization. The new Grell scheme is used for cumulus parameterization (Grell & Freitas, 2014). We use the WRF Single Moment 5-class cloud microphysics scheme with ice and snow parameterizations allowing for mixed-phase processes and super-cooled water (Hong et al., 2004). The Rapid Radiative Transfer Model (RRTMG) for both SW and LW radiation is used for radiative transfer calculations (Iacono et al., 2008; Mlawer & Clough, 1998; Mlawer et al., 1997). Only the aerosol direct radiative effect is accounted for.

WRF-Chem is a tropospheric model, therefore we had to modify the code to be able to simulate the evolution of a volcanic cloud in the stratosphere. We developed a volcanic emission scheme to inject multiple species to initiate the cloud evolution, extended the calculation domain vertically until the top of the stratosphere at 1 hPa, implemented the sulfur cycle and ash calculations in the stratosphere, included gravitational settling of sulfate aerosols since it is important in the stratosphere, corrected the WRF-Chem numerical scheme for gravitational settling to avoid an artificial mass gain, modified the radiative scheme to account for SO_2 absorption both in SW and LW, included radiative effects of SO_2 and aerosols (both ash and sulfate aerosols) in the photolysis rates calculations, and implemented on-line instantaneous radiative forcing

calculations for SO_2, ash, and sulfate aerosols (Ukhov et al., 2021; Ukhov, Mostamandi, da Silva, et al., 2020; Ukhov, Mostamandi, Krotkov, et al., 2020).

2.1. Atmospheric Chemistry and Aerosols

To calculate gas-phase chemistry, we use the Regional Atmospheric Chemistry Mechanism (RACM) with 77 species and 237 reactions, including 23 photolytic reactions (Stockwell et al., 1997). The heterogeneous chemical reactions are not included. The most important photochemical reaction for the formation of a volcanic cloud is the photodissociation of ozone. It generates atomic oxygen that reacts with water to create OH. OH, in turn, reacts with SO_2 to produce sulfuric acid, H_2SO_4. The production of OH is calculated interactively within RACM and its concentration is provided to the aerosol module, Georgia Tech/Goddard Global Ozone Chemistry Aerosol Radiation and Transport model (GOCART) (Chin et al., 2009, 2014, 2002). GOCART calculates SO_2 to sulfate (SO_4) oxidation by OH and treats both sulfate and ash aerosols.

GOCART uses a bulk approach for sulfate aerosols, that is, only SO_4 concentrations and mixing ratios are calculated and presented. It is assumed that sulfate aerosol droplets are formed instantaneously. All SO_4 is in particle form. It is mixed with water to form sulfate aerosols. Sulfate aerosol wet radius is defined by the initially prescribed SO_4 dry radius, relative humidity RH, and hygroscopic parameter k (Aquila et al., 2012; Petters & Kreidenweis, 2007). Following Aquila et al. (2012), we assume that for sulfate particles, hygroscopic parameter $k = 1.19$.

To calculate sulfate aerosol optical properties and gravitational settling we assume, based on previous observations (Borrmann et al., 1995; Deshler et al., 1993; Pueschel et al., 1994; Russell et al., 1996) that SO_4 number-density size distribution can be approximated by two lognormal modes, Aitken and Accumulation. Aitken mode has a median radius $r_1 = 0.09$ μm and the geometric width $\sigma_1 = 1.4$. The accumulation mode has a median radius $r_2 = 0.32$ μm and the geometric width $\sigma_2 = 1.6$. We assume that accumulation mode comprises 95% of the aerosol mass, and Aitken mode—5%. We refer to this size distribution setting as Size Distribution A. To test the sensitivity to these assumptions we also conduct simulations with the significantly different sulfate aerosol size distribution that we denote, as Size Distribution B: $r_1 = 0.05$ μm, $\sigma_1 = 1.7$, $r_2 = 0.4$ μm, $\sigma_2 = 2.0$, with Aitken and Accumulation mode mass fractions 25% and 75%, respectively. The refractive index of sulfate particles depends on sulfuric acid concentration within the droplets defined by temperature and relative humidity (Stenchikov et al., 1998). Ash particles are mostly silicates, so we use the GOCART dust aerosol option to mimic volcanic ash. To calculate ash microphysics, we use a sectional microphysical model with five discrete ash-bin(i), $i = 1, 2, 3, 4$, and 5 with the radius edges at 0.1, 1, 1.8, 3.0, 6.0, and 10.0 μm, respectively. It is assumed that within each bin ash particles have the same physicochemical and optical characteristics. Their Complex Refractive Index RI = 1.550 + i0.001 has been chosen to approximate ash optical properties (Pollack et al., 1973; A. Vogel et al., 2017). We do not account for ash agglomeration. In WRF-Chem, a parameterized Mie theory (Ghan & Zaveri, 2007) is employed to calculate the aerosol optical properties assuming (only for calculating optics) that sulfate and ash aerosols are internally mixed.

2.2. Gravitational Settling

The gravitational settling of dust, which in our case mimics ash, is accounted for in WRF-Chem, but the sulfate aerosol droplets in the troposphere are smaller than 0.2 μm and therefore, in the troposphere, conventional WRF-Chem/GOCART accounts only for dry (turbulent) and wet sedimentation of sulfate aerosols. Because in the stratosphere the sulfate aerosol droplets are bigger and air density is lower than in the troposphere, gravitational settling becomes the leading deposition process. Therefore, we implement the gravitational settling of sulfate aerosols in WRF-Chem similar to that Aquila et al. (2012) did in Goddard Earth Observing System Version 5 (GEOS-5) general circulation model.

We also correct the calculations of aerosol gravitational settling both for sulfate aerosols and ash within WRF-Chem. It was originally coded to calculate aerosol gravitational settling from the relatively thin surface layer and did not account properly for the change of air-density in altitude. This is not so detrimental near the surface but causes severe problems in the stratosphere where, within our domain, air density changes by two orders of magnitude. The calculation of gravitational settling velocities is expanded to account for low

stratospheric air-densities using the approximation for settling velocities (Kasten, 1968). The modification of the gravitational settling numerical scheme is discussed in detail in Ukhov et al. (2021).

For the ash gravitational settling, the terminal velocities are calculated for the mean volume radii within each bin size, while the sulfate particles in accumulation mode are settled assuming their wet mean radius of volume size distribution of the accumulation mode. It is assumed that sulfate aerosol density is 1,800 kg/m^3. Ash density is assumed to be 2,500 kg/m^3 for the first bin and 2,650 kg/m^3 for bins from 2 to 5.

2.3. Effect of Aerosols and SO_2 on Photolysis Rates

To calculate actinic fluxes and photolysis rates we use the Madronich (1987) F-TUV parameterization. A primary source of OH is ozone photolysis which is driven by UV actinic fluxes. Aerosols, both sulfate and ash as well as SO_2, reduce UV actinic flux and slow down the photochemical conversion of SO_2 to SO_4 (Bekki, 1995; Bekki et al., 1996; Dickerson et al., 1997; Mok et al., 2016). In our WRF-Chem setting, we modify the F-TUV scheme used for the actinic flux (and photolysis rates) calculations so that the F-TUV module now interactively accounts for aerosols and trace gases, including SO_2. The SO_2 absorption cross-section at 0.106–0.404 μm is obtained from Manatt and Lane (1993). For more details on the effect of SO_2 and aerosols on O_3 photolysis see Osipov et al. (2020).

2.4. Radiation Transfer

For radiation transfer calculations in WRF-Chem, we choose the Rapid Radiative Transfer Model (RRTM) for SW and LW (Iacono et al., 2008; Mlawer & Clough, 1998; Mlawer et al., 1997). SO_2 is optically active in SW and LW, but because SO_2 concentration is usually low, radiative transfer codes do not account for the SO_2 effect. However, SO_2 concentration in a volcanic cloud could initially exceed a few ppmv, so the radiative effect from SO_2 might be significant. Therefore, in cooperation with the developers of RRTM from Atmospheric and Environmental Research (AER), we modified the latest AER public releases of RRTMG_LW_v4.85 and RRTMG_SW_v3.9 (Iacono et al., 2008). The modified RRTMG_LW and RRTMG_SW codes are implemented in WRF-Chem to allow the accurate calculation of radiative fluxes and heating rates for profiles containing SO_2 with concentrations <2 mg m^{-3}. The following spectral bands are modified to allow accurate calculations of the radiative effect of SO_2:

- RRTMG_LW band 2 (350–500 cm^{-1})
- RRTMG_LW band 3 (500–630 cm^{-1})
- RRTMG_LW band 8 (1,080–1,180 cm^{-1})
- RRTMG_LW band 9 (1,180–1,390 cm^{-1})
- RRTMG_SW band 27 (29,000–38,000 cm^{-1})

In RRTMG_LW, we split band 9 into two intervals (1,180–1,330 and 1,330–1,390 cm^{-1}), which results in 17 total LW spectral bands. The accuracy of the modified codes is evaluated with respect to the flux and heating rate computed by a reference Line-by-Line code for multiple SO_2 profiles and a set of atmospheric conditions.

3. Experimental Setup

The cloud of volcanic products from the 1991 Pinatubo eruption encircled the Earth in about 22 days (Bluth et al., 1992), but it took from 3 to 4 months for it to reach 60°N (Long & Stowe, 1994; McCormick et al., 1995; Russell et al., 1996). Therefore, to study the first 3 months of the evolution of this cloud we choose the latitudinal belt domain (30°S–60°N) with periodic boundary conditions in longitude similar to that used in the quasi-global WRF-Chem setting in Hu et al. (2016), see Figure 1. We use a 25 × 25 km^2 horizontal grid (1,500 × 444 grid points) and 53 vertical levels. The top of the model has been raised to 1 hPa to account for dynamical processes in the stratosphere. For numerical stability, we choose time step in the range of 20–45 s.

The meteorological initial and boundary conditions for WRF-Chem are calculated using the ERA-Interim reanalysis product on 72 model layers spread up to 0.01 hPa (Dee et al., 2011). To better reproduce the

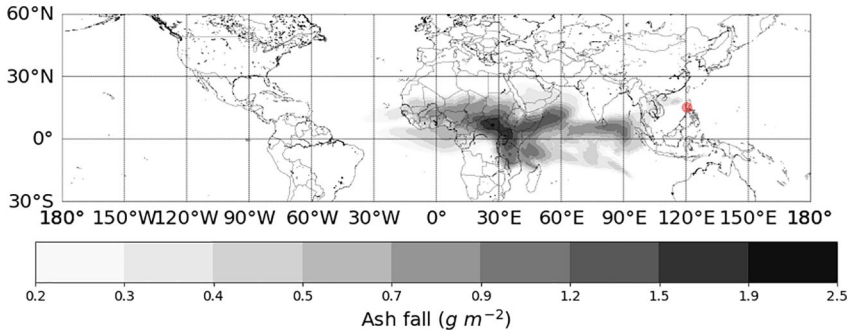

Figure 1. Simulation domain marked with Mt. Pinatubo's geographic location in western Luzon Island in the Philippines (15.1429°N, 120.3496°E). Gray shading shows accumulated for 3 months (June 15–September 15) deposited ash (0.1 μm < r < 10 μm) mass (g/m^2) in the reference run FW17S111A10 (see Table 1).

equatorial stratospheric circulation at the time of the 1991 Pinatubo eruption, the wind Spectral Nudging is applied (Miguez-Macho et al., 2004). We nudge the three longest longitude and one longest latitude's Fourier harmonics of horizontal wind components above the boundary layer (>5 km) toward the ERA-Interim wind field with a characteristic time of 3 h. This allows for capturing the observed QBO phase. For consistency, the prescribed sea surface temperature from ERA-Interim reanalysis is used. In the course of the sensitivity study, simulations with 100 km grid spacing (see Table 1) are also conducted.

In our runs, we turned off all surface aerosol and gaseous emissions (e.g., dust, SO_2) to avoid interference with the tropospheric effects. As we conduct simulations in the latitude band, the lateral boundary conditions ensure that the meteorological fields are well reproduced. We could even correctly simulate the landfall of typhoon Yunya that hit the Philippines on June 11–17, 1991.

The Pinatubo eruptive activity began on June 12, but the strongest injection happened on June 15 from 0141 to 2300 UTC, with the largest volume of ejecta occurred during 9 h from 0430 to 1400 UTC (Bluth et al., 1992, 1993; Fero et al., 2009; Guo, Bluth, et al., 2004; Holasek et al., 1996). To mimic the Pinatubo eruption of 1991, we emit eruption products (SO_2, ash, water vapor, sulfate) in a "small" volume of 125 × 75 × 4 km^3 (in longitude, latitude, and height, respectively) centered above the tropical tropopause at 17 km height and geographic coordinates of Mt. Pinatubo (15.1429°N, 120.3496°E) with a constant mass rate in time. In the course of a sensitivity study, we also consider emission at 20.5 and 24 km height or in a "large" volume of 2,125 × 525 × 4 km^3 (see Figure 2 and Table 1). We start the volcanic injection on June 15, 1991, at 0000 UTC and continue injecting with constant rate for 24 h. The vertical profile of the emission rate within the four model vertical layers (each 1-km thick) is parabolic; the fractions of mass injected in each layer are 20%, 30%, 30%, and 20% from the bottom to the top of the emission volume, respectively (Figure 2).

Following Guo, Bluth, et al. (2004), we emit 17 Mt of SO_2. It is conventionally assumed that a volcanic cloud initially contains no SO_4, as gaseous oxidation of SO_2 requires at least 2 weeks. Also, SO_4 generated in the liquid phase could not make it through the cold tropopause layer. However, this does not completely exclude the possibility that some SO_4 is present in the volcanic cloud from the beginning (Dhomse et al., 2014; Guo, Rose, et al., 2004). For example, Zhu et al. (2020) showed that heterogeneous reactions on ash particles' surfaces could quickly produce sulfate. LeGrande et al. (2016) demonstrated that volcanic water injection also accelerates the SO_2 oxidation at the early development of the volcanic cloud. Therefore, to mimic this effect in the course of the sensitivity study, we conduct runs with and without initial SO_4 injection.

Injected ash has an immediate and large radiative heating effect (Gerstell et al., 1995; Niemeier et al., 2009). Guo, Bluth, et al. (2004) estimated that the mass of emitted fine ash was 80 Mt. Here, we follow Niemeier et al. (2009) who assumed that Pinatubo injected 100 Mt of fine ash with a log-normal number-density size distribution which has a median radius of 2.4 μm and the geometric width of 1.8. As the WRF-Chem ash-bins cover only particle radii <10 μm, we cut the large-radii tail of this distribution, assuming the particles larger than 10 μm have a short lifetime with respect to gravitational settling and are removed quickly during the injection and initial dispersion of volcanic cloud. The remaining mass of fine ash with radii <10 μm is 75 Mt, close to that suggested by Guo, Rose, et al. (2004). The ash mass is distributed within the GOCART's

Table 1
Numerical Experiments

Experiment name: Grid spacing—**F**ine/**C**oarse With or without water vapor injection—**W**et/**D**ry Height of injection—**17**/**24**/**N**one Injection volume size—**L**arge/**S**mall/**N**one	**SO_2** Radiative effect is on/off—**1**/**0**	**Ash** Radiative effect is on/off—**1**/**0**/**N**one	**Sulfate (SO_4)** Radiative effect on/off—**1/0** Size distribution—**A**/**B**/**N** Gravitational settling on/off—**1**/**0** Initially present in the volcanic cloud: Yes/no—**1**/**0**
FDNN000N00, Control Experiment	None	None	None, Section 4.2–4.5
FW17S111A10, Whole Physics Reference Experiment	1	1	1, A, 1, 0, Sections 4.2–4.6
FW17S000A10, 17 km, Small	0	0	0, A, 1, 0, Sections 4.2 and 4.3
	No rad. feedback	No rad. feedback	No rad. feedback
FW17S1N1A10, 17 km, Small	1	None—No ash	1, A, 1, 0, Section 4.4
FW17S121A10, 17 km, Small	1	2, Bin(5) removed	1, A, 1, 0, Section 4.6
FW17S131A10, 17 km, Small	1	3, All bins halved	1, A, 1, 0, Section 4.6
FW17S111B10, 17 km, Small	1	1	1, B, 1, 0, Sections 4.3 and 4.4
FW17L111A10, 17 km, Large	1	1	1, A, 1, 0, Section 4.3 Large injection volume
FW17S111A00, 17 km, Small	1	1	1, A, 0, 0, Section 4.4 SO_4 settling is turned off
FW17S111A11, 17 km, Small	1	1	1, A, 1, 1, Sections 4.4 and 4.5 Injected 4 MT SO_4 Total S mass = 8.5 Mt
CW17S111A10, 17 km, Small coarse-resolution run	1	1	1, A, 1, 0, Section 4.3 100 km grid spacing
FD24S111A10, 24 km, Small	1	1	1, A, 1, 0, Sections 4.4 and 4.5 No water vapor injection
FW24S111A10, 24 km, Small	1	1	1, A, 1, 0, Section 4.5
FW20S111A10, 20.5 km, Small	1	1	1, A, 1, 0, Section 4.6

Note. The indexes in the experiment title define spatial resolution, volcanic water injection, emission height and volume (Large 2,125 × 525 × 4 km^3 or Small 125 × 75 × 4 km^3), whether radiative feedback of SO_2, ash, and sulfate is active, sulfate aerosols size distribution, whether sulfate gravitational settling is turned on and SO_4 is initially injected. The employed Sulfate Aerosol Number-density Size Distributions are as follows: A: Aitken mode $r_1 = 0.09$ μm, $\sigma_1 = 1.4$; fraction = 5% Accumulation mode: $r_2 = 0.32$ μm, $\sigma_2 = 1.6$; fraction = 95%. B: Aitken mode $r_1 = 0.05$ μm, $\sigma_1 = 1.7$; fraction = 25% Accumulation mode: $r_2 = 0.40$ μm, $\sigma_2 = 2.0$; fraction = 75%.

five bins. The ash-bins from 1 to 5 comprise 0.1%, 1.5%, 9.5%, 45%, and 43.9% of this mass, respectively. The estimates of ash mass and injection height are uncertain (Gouhier et al., 2019; Mastin et al., 2009). The accumulated radiative effect of ash also depends on its size distribution. Large ash particles with $r > 3$ μm settle down quickly, but smaller particles with $r < 3$ μm could stay in the stratosphere much longer producing prolonged radiative heating.

Water vapor in the volcanic cloud affects both the radiative heating of the cloud and its chemical evolution (Bekki, 1995; LeGrande et al., 2016; Pinto et al., 1989). The mass of entrained water from the troposphere and "volcanic" water, brought into the stratosphere by eruptive jet and co-ignimbrite convection, is of the order of 100 Mt (Dessler et al., 2014; Guo, Bluth, et al., 2004; Guo, Rose, et al., 2004; Joshi & Shine, 2003). If retained in the stratosphere, this could cause a more than 10% increase of stratospheric water, which was never detected in that amount. In our experiments, we inject 100 Mt of water vapor, but because it is subjected to phase transformations, a significant portion of it is condensed and deposited. In the course of the sensitivity study, we conduct runs with and without water injection.

It was observed that the Pinatubo eruption of 1991 caused about 5% of tropical ozone depletion (Angell, 1997; Stenchikov et al., 2002). As we simulate the initial stage of a volcanic cloud evolution when

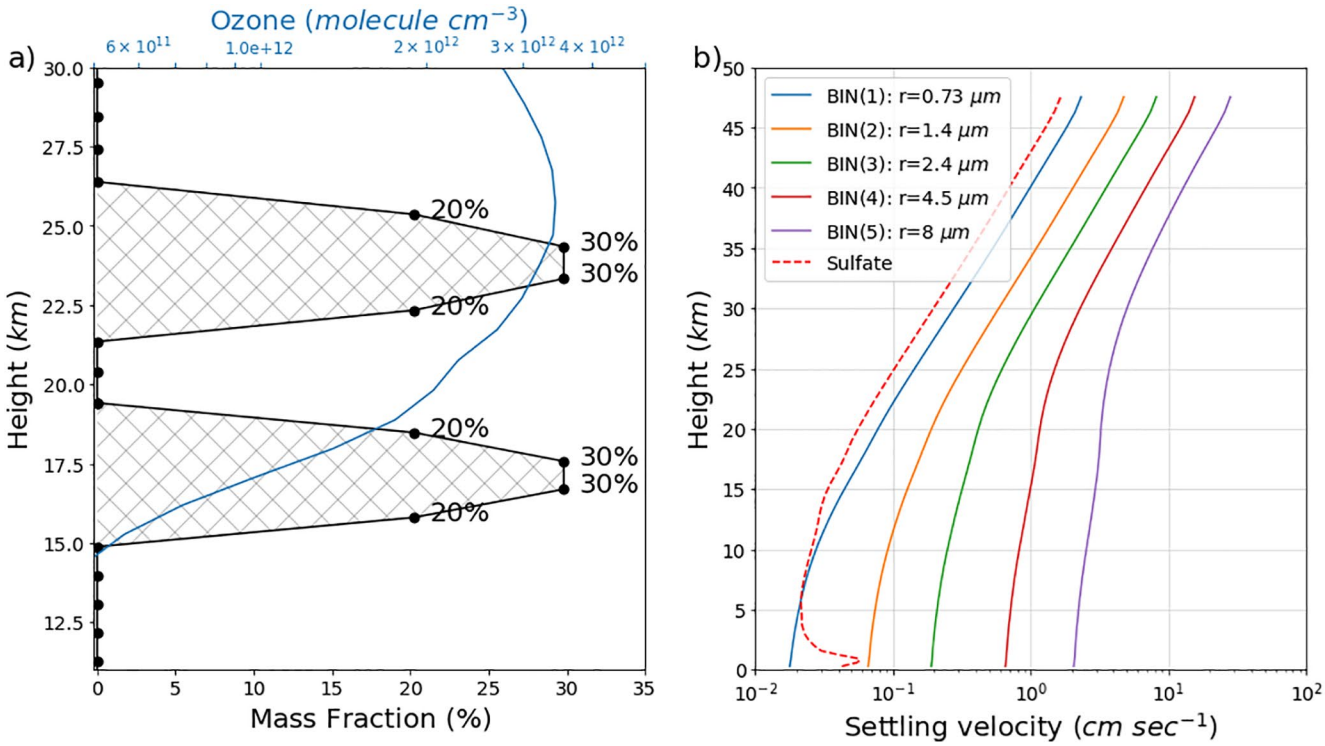

Figure 2. (a) Vertical distribution of injected ash, SO_2, and volcanic water vapor masses released at 17 or 24 km into four 1-km deep model layers with the fractions (%) of mass per layer shown on the plot. The blue line depicts the prescribed climatological profile of ozone (mol cm^{-3}). (b) Gravitational settling velocities (cm s^{-1}) as a function of height for five ash bins and sulfate aerosols as implemented in WRF-Chem averaged over the horizontal domain.

stratospheric ozone is not yet wholly responsive, the ozone profile from the top until 300 hPa is kept climatological using WRF-Chem's upper boundary condition option (Figure 2).

To quantify the role of radiative feedback and sensitivity of the volcanic cloud evolution to the injection's height and chemical composition, we conduct experiments with and without radiative feedback of eruption products. We also test sensitivity to the size distribution of sulfate aerosols and the presence of ash. The total list of experiments is presented in Table 1. The experiments start on June 5, 1991, 10 days before the eruption, leaving time for the mesoscale spin-up, and they continue for three months until the volcanic cloud reaches the lateral boundaries of the domain. The 10-day spin-up is excluded from the analysis. We calculate radiative heating associated with each component on-line. All experiments are performed with 25-km grid spacing except CW17S111A1, which was calculated on the 100 × 100 km^2 horizontal grid to quantify the model sensitivity to the spatial resolution.

4. Results

Our main focus in this study is on the volcanic cloud dynamics driven by ash, sulfate aerosols, and SO_2 radiative heating. Volcanic products are injected simultaneously in the same volume with identical normalized injection rates. But during a 24-h injection, their spatial distributions within the plume evolve. The stratospheric winds spread all debris horizontally to a few thousand km. The SO_2 and ash layers are heated and move up slightly, but ash particles are falling down, quickly filling the column from 19 to 9 km well below the SO_2 layer. Injected water vapor condenses and is removed from the stratosphere. A small amount of hydrometeors remain in the volcanic cloud consistent with observations (Guo, Rose, et al., 2004).

4.1. Radiative Heating and Lofting in a Fresh Dense Volcanic Cloud

To demonstrate the impact of radiative feedback on dynamics, we calculate radiative heating in a very fresh volcanic cloud using a stand-alone column radiative transfer model similar to the methods used in early

studies (Lary et al., 1994; Zhong et al., 1996). The spatial distributions of the optically active components correspond to the state of the volcanic cloud on the second day after the beginning of the eruption. Figure 3 shows the diurnal average radiative heating rates associated with the different eruption products, assuming that all volcanic materials are uniformly distributed within the 2,125 × 525 × 4 km^3 volume centered at 17 km height (15–19 km), with the exception of ash, which loads the column 9–19 km. The volcanic cloud comprises the initial amounts of SO_2 and ash (17 Mt and 75 Mt, respectively). All injected water vapor is removed, since the injection volume is at the cold point where relative humidity RH = 100%. We assume that only 1 Mt of ice remains in the volcanic cloud. We also assume that 1 Mt of SO_4 is initially present in the same volume as SO_2 to test its contribution in the volcanic cloud radiative heating (Guo, Rose, et al., 2004). The heating rate generally scales with the magnitude of the injection of a particular constituent. For example, if we inject 4 Mt of SO_4, its heating rate quadruples in comparison with the 1 Mt injection of SO_4, shown in Figure 3.

The calculations are performed with the June insolation at 15°N for the equatorial atmospheric profile using the stand-alone RRTM (Iacono et al., 2008; Mlawer & Clough, 1998; Mlawer et al., 1997). It is the same radiative scheme that we use in WRF-Chem. The column model is described in Osipov et al. (2015) and was later updated by including the radiative effects of SO_2 (Osipov et al., 2020). Optical properties of sulfate aerosols, ash, and ice aerosols (extinction, single scattering albedo, and phase function) are calculated for the same size distributions which we use in the WRF-Chem simulations assuming the sphericity of particles and using analytic Mie solution. The chemical composition of the atmosphere is prescribed according to monthly climatology derived from the Global Modeling Initiative model output (Douglass et al., 1999; Strahan et al., 2011). Lower boundary conditions assume a Lambertian reflection with surface albedo parametrized after Jin et al. (2004). Figure 3a depicts the vertical distributions of volcanic cloud ingredients. Figure 3b shows that ash warms the cloud the most (20 K/day). Sulfate aerosols, SO_2, and ice heat the volcanic cloud quite significantly (5.0, 2.5, and 1.75 K/day, respectively) but much less than ash. Heating rates are high because the volcanic cloud is concentrated. When it begins to become diluted, these heating rates decrease. Typhoon Yunya could affect LW heating of the volcanic cloud, but it is absent in our 1-D simulations. The effect of initial injection of SO_4 is further explored in Section 4.4.

Radiative heating forces the volcanic cloud to climb over the vertical gradient of potential temperature (θ). In the lower stratosphere

$$d\theta \,/\, dz = 30\ \mathrm{K/km}$$

The vertical velocity w that balances radiative heating of $Q = 20$ K/day could be calculated using thermodynamic considerations

$$w = \frac{Q \times \theta}{T \times d\theta \,/\, dz}. \tag{1}$$

Assuming that above the tropical tropopause the average potential temperature $\theta = 300$ K and conventional temperature $T = 200$ K we get

$$w = 1\ \mathrm{km/day}$$

which, as we will see below, fits well to the model calculated volcanic cloud rising velocity during the first week after the eruption.

The heating rates in Figure 3 are in agreement with the previous estimates of the radiative effect of SO_2. For example, Lary et al. (1994) found that in the lower stratosphere, SO_2 with a mixing ratio of a few ppmv absorbs the 0.180–0.36 μm SW radiation and causes about 0.25–0.3 K/day stratospheric heating. Note that SO_2 mixing ratios in our 1-D simulation and respectively SO_2 heating rates in Figure 3 are both an order of magnitude larger than in Lary et al. (1994). Although below the volcanic cloud the UV actinic flux and ozone photolysis rate are attenuated by 90%, a volcanic cloud injected at 17 km overlaps only with the bottom of the ozone layer where attenuation of photolysis rates does not exceed 40% (Figure 3c).

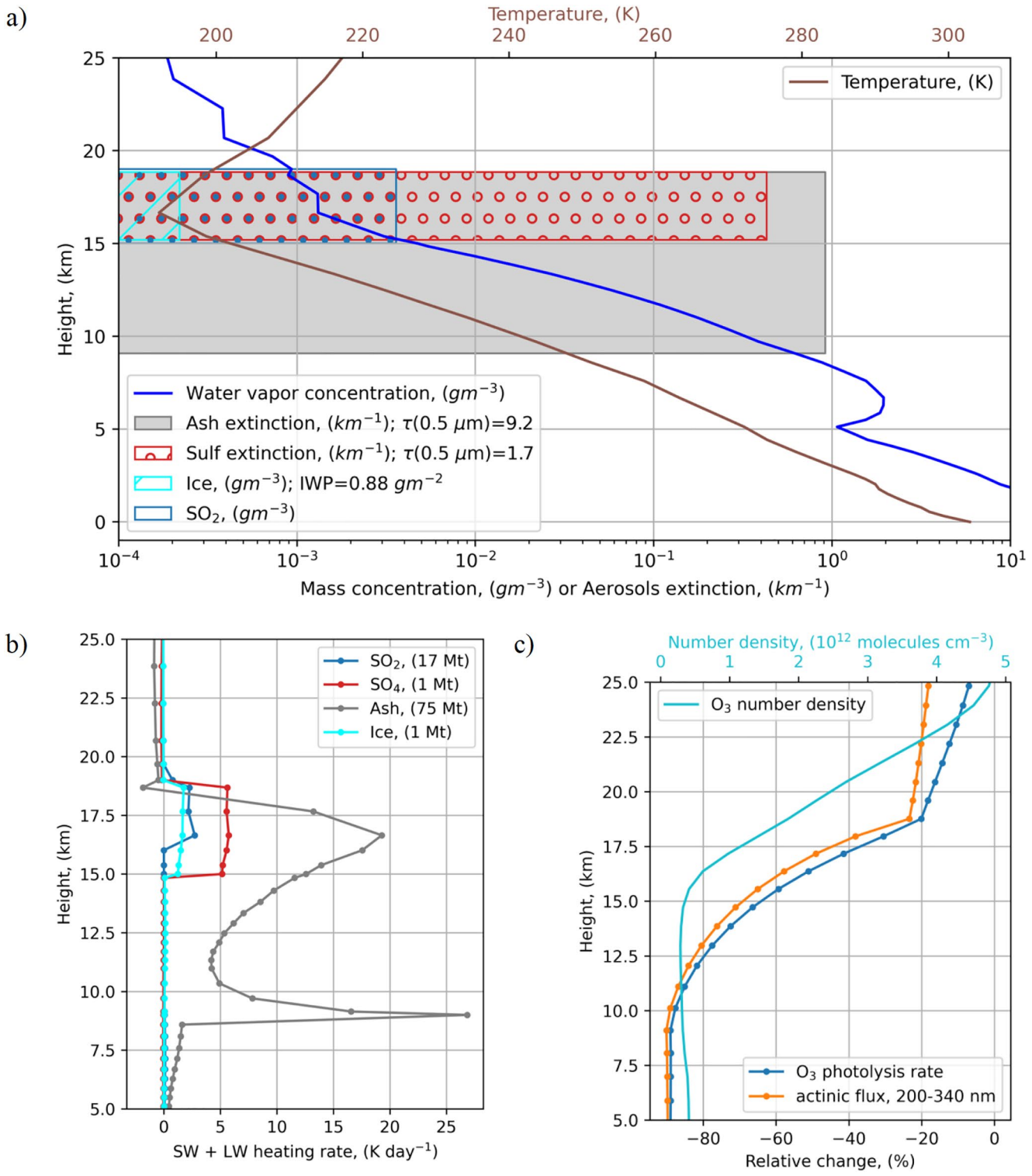

Figure 3. (a) Concentrations (g m^{-3}) of SO_2 and ice; extinctions (km^{-1}) of ash, and sulfate aerosols, τ denotes the optical depth of ash and sulfate aerosols, and IWP—ice water path (g m^{-2}) used to parameterize the ice radiative properties following Ebert and Curry (1992). (b) Diurnal average SW + LW heating rates (K/day). (c) O_3 number-density (10^{12} cm^{-3}), and relative changes (%) of diurnal average UV actinic flux and ozone photolysis rates caused by eruption products (ash, SO_2, and sulfate aerosols).

4.2. Volcanic Cloud Dynamics

In our simulations, we use a bulk aerosol model for sulfate that assumes fixed sulfate aerosol particle size distribution. It is a simplification, which is inevitable in bulk aerosol models. We know that in the Pinatubo volcanic cloud, sulfate particles grow due to coagulation and their effective radius reaches a maximum of 0.5–0.6 μm in 6 months after the eruption, and then decreases due to gravitational settling of large particles (Russell et al., 1996; Stenchikov et al., 1998). However, as we show below, during the first 3 months the sensitivity of volcanic cloud dynamics to sulfate aerosol size distribution is moderate. Therefore, this simplification is warranted.

We consider the FW17S111A10 run as most physically consistent with observations and therefore evaluate sensitivities with respect to it (see Table 1). We further refer to it as a whole physics reference experiment. The control experiment, FDNN000N00, does not have any volcanic emissions. Figure 4 compares the results from the FW17S111A10 and FW17S000A10 experiments with and without the volcanic cloud radiative feedback. It presents the time evolution of the area-averaged and volume integrated characteristics of the volcanic cloud. The mass of generated SO_4 (integrated over the entire 3-D domain) and the equatorial stratospheric aerosol optical depth (SAOD) reach their maximums by the end of August, which is consistent with SAGE filled observations (Thomason & Peter, 2006), see Figures 4a and 4b. We further refer to this data set as SAGE/ASAP. SAGE is a limb viewing instrument that measures aerosol extinction in the stratosphere at different altitudes.

We also show in Figure 4b the total aerosol optical depth at 0.63 μm from the Advanced Very High-Resolution Radiometer (AVHRR; Long & Stowe, 1994). AVHRR probably more realistically depicts the temporary evolution of SAOD than SAGE, which was saturated during the first few weeks after the eruption. AVHRR is a nadir viewing instrument that measures the optical depth of a whole atmospheric column. To calculate SAOD using AVHRR observations, we have to remove a tropospheric optical depth estimated using an average for 5 years (1994–1998) not affected by volcanic eruptions. This procedure could introduce uncertainty that is difficult to quantify. For example, AVHRR SAOD is visibly higher than that from SAGE.

Since GOCART only coarsely parameterizes sulfate aerosol microphysics and does not account for heterogeneous processes on ash surfaces, the SO_2 to SO_4 conversion and growth (decrease) of the SO_4 (SO_2) mass is slower than observed (Bekki et al., 1996; LeGrande et al., 2016). The equatorial zonal mean profile of SO_2 mixing ratios in our simulations in September of 1991 (Figure 4c) shifts up in comparison with the observed one (Read et al., 1993). The simulations overestimate SO_2 mixing ratios above 15 hPa partly because of SO_2 conversion to SO_4 is slow. With radiative feedback, the maximum values of SO_4 mass and SAOD in the reference experiment FW17S111A10 are two times larger than in the experiment without radiative feedback FW17S000A10, because of quicker mass loss through the tropopause of both SO_2 and SO_4 in the latter experiment. This sensitivity is probably enhanced by the proximity of the tropopause in our 17-km injection setting.

Figure 4d shows the time evolution of the masses of ash in different size-bins integrated over the entire 3-D domain. Large ash particles from bins 4 and five quickly settle down. After a month, only 10% of total ash mass (mostly from bin 3 with particle's radii < 3 μm) remains in the atmosphere. The coarsest ash bin(5) with $6 < r < 10$ μm comprises about half of ash mass deposits almost completely in 2 weeks. However, the finest ash in bins 1 and 2 with $0.1 < r < 1.8$ μm can stay in the volcanic cloud until the middle of August, but contain little mass and have negligible optical depth (Figure 4b). In the simulations, ash was injected at a height of 17 km. At this altitude, the gravitational settling velocity for particles in the coarsest bin is about 3 km/day, so it takes 5–6 days until they reach the ground and leave the atmosphere as in Figure 4d. In the AVHRR observations, the rate of ash mass removal is consistent with that in bin(5) but the ash mass decreases immediately after the injection. It means that in reality ash particles fill the entire atmospheric column and start depositing to the ground immediately after the eruption, or collective deposition causes very fast ash fallout (Gouhier et al., 2019). Therefore, the observed ash mass reduction does not experience a delay that is seen in simulations. It is also possible that the instrument cannot see ash in the troposphere below clouds.

Because of low temperatures at a cold point at 17 km, almost all the injected water condenses and deposits as ice and snow. Little volcanic water rises above 50 hPa to reach the middle stratosphere (Figure 4e).

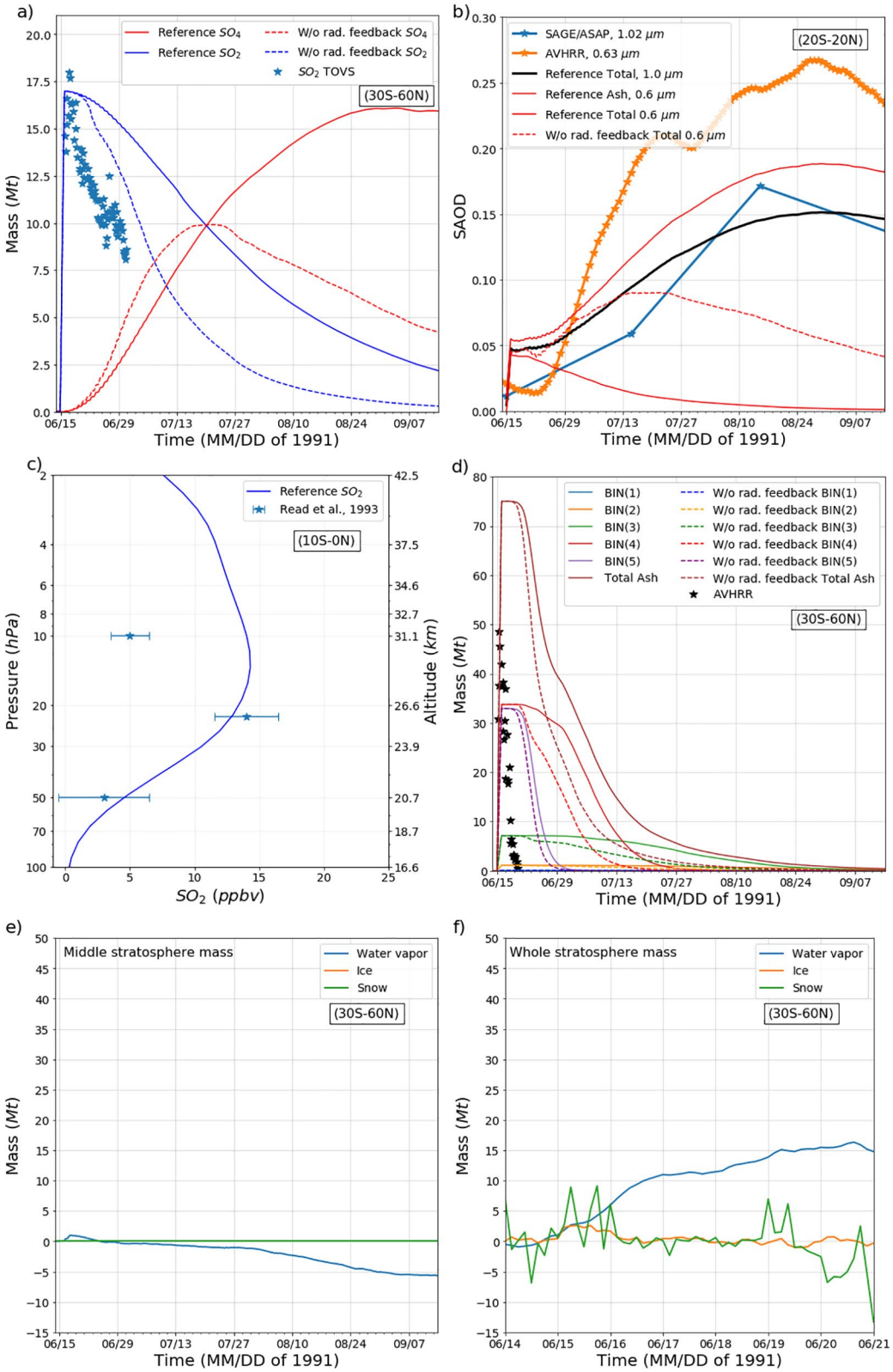
a)
Reference SO_4
Reference SO_2
W/o rad. feedback SO_4
W/o rad. feedback SO_2
SO_2 TOVS
(30S-60N)
Mass (Mt)
Time (MM/DD of 1991)
b)
SAGE/ASAP, 1.02 μm
AVHRR, 0.63 μm
Reference Total, 1.0 μm
Reference Ash, 0.6 μm
Reference Total 0.6 μm
W/o rad. feedback Total 0.6 μm
(20S-20N)
SAOD
Time (MM/DD of 1991)
c)
Reference SO_2
Read et al., 1993
(10S-0N)
Pressure (hPa)
Altitude (km)
SO_2 (ppbv)
d)
BIN(1)
BIN(2)
BIN(3)
BIN(4)
BIN(5)
Total Ash
W/o rad. feedback BIN(1)
W/o rad. feedback BIN(2)
W/o rad. feedback BIN(3)
W/o rad. feedback BIN(4)
W/o rad. feedback BIN(5)
W/o rad. feedback Total Ash
AVHRR
(30S-60N)
Mass (Mt)
Time (MM/DD of 1991)
e)
Middle stratosphere mass
Water vapor
Ice
Snow
(30S-60N)
Mass (Mt)
Time (MM/DD of 1991)
f)
Whole stratosphere mass
Water vapor
Ice
Snow
(30S-60N)
Mass (Mt)
Time (MM/DD of 1991)

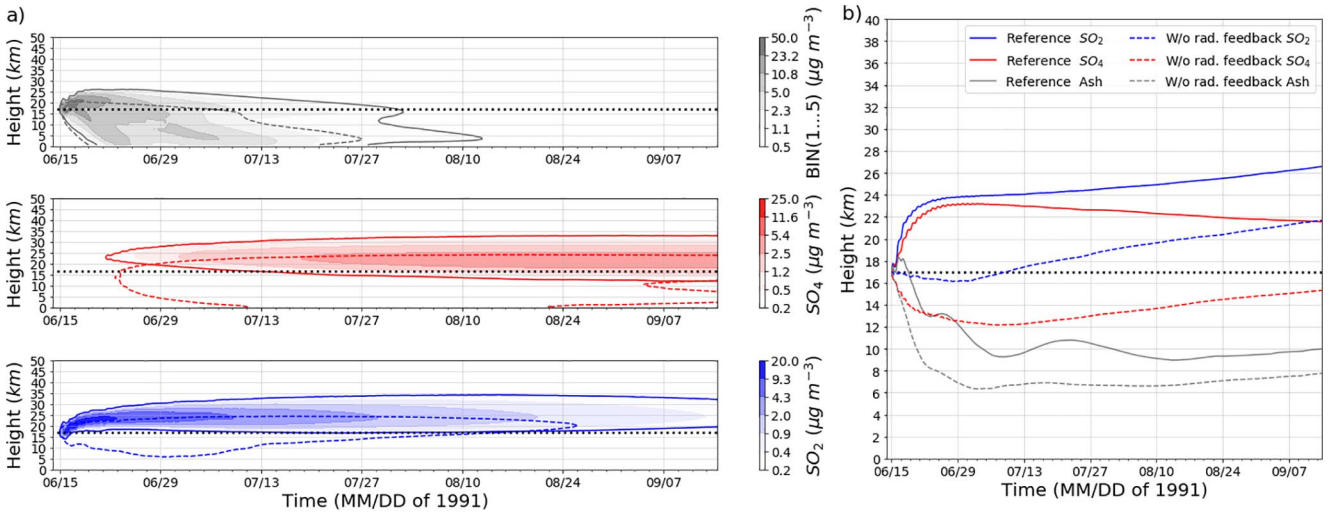

Figure 5. (a) Hovmöller diagrams of SO_4 (red), SO_2 (blue), and ash (gray) concentrations (μg/m^3) averaged over the 30°S–60°N latitude belt as a function of time and height. Solid contour lines and shading correspond to the reference run FW17S111A10 with sulfate aerosols, ash, and SO_2 radiative feedback. Dashed contour lines correspond to the FW17S000A10 run without radiative feedback. (b) The heights (km) of the center of mass of SO_4 (red), SO_2 (blue), and ash (gray) clouds. Solid contour lines correspond to the FW17S111A10 run with sulfate aerosols, ash, and SO_2 radiative feedback. Dashed lines correspond to the FW17S000A10 run without volcanic cloud radiative feedback. Dotted black line shows the 17-km injection height.

Figure 4f shows that less than 1 Mt of ice remains in the volcanic cloud by June 16, 1991, consistently (Guo, Rose, et al., 2004). However, when the injection phase is over, the water vapor content in the lower stratosphere above 100 hPa grows slowly due to heating of the tropopause, initially by volcanic ash, and after 2 weeks by sulfate. In our simulation, the amount of water in the lower stratosphere after the eruption increases by almost 15 Mt (Figure 4f). In the middle stratosphere above 50 hPa, after the initial increase by about 1 Mt, the total water content decreases, as it is consumed in the SO_2 oxidation (see Figure 4e). Along with the relatively fast horizontal transport, eruption products in the tropical lower stratosphere also move up in the ascending branch of BD circulation and loft depending on their radiative heating (Figure 5a). Aerosol particles (sulfate and ash) are subjected to gravitational settling.

Figure 5a shows the ash, SO_2, and SO_4 concentrations averaged over the entire domain as a function of altitude z and time t in the reference experiment (FW17S111A10), and in the experiment without radiative feedback of SO_2, sulfate aerosols, and ash (FW17S000A10). Figure 5b shows the height of the center of mass h_α of SO_2, SO_4, and ash clouds in both FW17S111A10 and FW17S000A10 experiments:

$$h_\alpha = \frac{\int_{\varphi_1}^{\varphi_2}\int_0^{2\pi}\int_0^{\infty} C_\alpha \times z \times a^2 \cos\varphi \times dz \times d\phi \times d\lambda}{\int_{\varphi_1}^{\varphi_2}\int_0^{2\pi}\int_0^{\infty} C_\alpha \times a^2 \times \cos\varphi \times dz \times d\varphi \times d\lambda}, \quad (2)$$

where $C_\alpha(\lambda,\varphi,z,t)$ is a concentration of SO_2, SO_4, or ash, a—radius of Earth, φ—latitude, λ—longitude, and φ_1, φ_2—southern and northern borders of the latitude belt (Figure 1).

Figure 4. Spatially integrated characteristics from the whole physics reference run (FW17S111A10, solid lines), and the run without radiative feedback (FW17S000A10, dashed lines) (a) Masses (Mt) of SO_2 and SO_4 integrated over the 30°S–60°N latitude belt, as a function of time. The TOVS retrievals of SO_2 mass are shown by markers (Guo, Bluth, et al., 2004). (b) Simulated Ash and Total (ash + sulfate aerosols) SAOD at 1.0 and 0.6 μm averaged over the 20°S–20°N latitude belt, as a function of time. The observed AVHRR at 0.63 μm (Long & Stowe, 1994) and SAGE at 1.02 μm (Thomason, 1992; Thomason et al., 2018; Thomason & Peter, 2006) 20°S–20°N mean SAODs are shown by orange and blue lines (respectively) with markers. The model diagnostics are averaged over the same overlapping areas where SAGE data are available. (c) Vertical profile of the simulated SO_2 mixing ratio (ppmv) (10°S–10°N average in the first half of September) compared with observations from (Read et al., 1993). (d) Masses (Mt) of ash in each of five bins and their total mass integrated over the 30°S–60°N latitude belt, as a function of time. The AVHRR retrievals of the mass of fine ash (diameters 0–15 μm) are shown by markers (Guo, Rose, et al., 2004). (e) The anomaly of the masses (Mt) of water vapor and hydrometeors in the middle stratosphere (above 50 hPa) with respect to the control run (FDNN000N00) integrated over the 30°S–60°N latitude belt, as a function of time. (f) Same as (e), but in the whole stratosphere above 100 hPa, shown for the first 6 days. AVHRR, Advanced Very High-Resolution Radiometer; SAGE, Stratospheric Aerosol and Gas Experiment; SAOD, stratospheric aerosol optical depth.

Because of the different gravitational settling velocities, the ash, SO_2 (which has zero settling velocity), and sulfate clouds already separate in altitude in the course of the initial injection. Despite ash and SO_2 being injected in the same volume, at the end of the injection phase the core of the ash cloud is well below the core of the SO_2 cloud (Figure 5b). In Figure 5a, ash and SO_2 are present from the beginning of the run. There are no sulfate aerosols in the fresh cloud, as it takes about 10 days to develop a significant amount of SO_4. The SO_2 oxidation is inhibited initially by the reduction of UV actinic fluxes in the volcanic cloud due to SO_2 and ash absorption. We will discuss the effect of initial SO_4 injection in Section 4.4.

The solid lines in Figure 5a depict the volcanic clouds' boundary in the reference experiment when radiative heating of ash, SO_2, and sulfate aerosols, both in SW and LW, is turned on. The dashed lines define the volcanic cloud boundaries when radiative heating is turned off. The threshold concentrations bordering the cloud correspond to the lowest value on the color bar. The same color and line-style conventions apply to Figure 5b. The SO_2 cloud moves up, driven by buoyancy generated by radiative heating of eruption products (see Figures 3 and 5). In a week, the SO_2 cloud lifts by 7 km (about 1 km/day). In the run, without volcanic cloud's radiative feedback (FW17S000A10) the stratospheric updrafts also move SO_2 and SO_4 up but much slower (20–30 m/day) than lofting (Figure 5b). The BD tropical uplift starts to be important in 2–3 months when thermal lifting diminishes. The top of the SO_2 cloud reaches 35-km while the center of mass climbs to 23 km. SO_2 is a gas and does not experience a gravitational settling, but it depletes due to converting into sulfate, which also affects the position of the SO_2 center of mass. In contrast, SO_4 cloud upward motion is restricted by gravitational settling of sulfate aerosols. The sulfate cloud initially overshoots to 23 km and then dilutes and descends when buoyancy generation reduces.

Despite the gravitational settling, the ash cloud rises initially by 1–1.5 km before descending quickly into the troposphere (Figure 5). In the experiment without heating feedback (dashed line in Figures 4 and 5), the SO_2 and SO_4 clouds end up 5–6 km lower than in the reference experiment, and significant sulfate mass is lost to deposition during the first 3 months. We discuss this effect in more detail below in Section 4.4.

4.3. Radiative Heating

Figure 6 shows daily mean SW, LW, and total (SW + LW) atmospheric heating rates caused by SO_2, sulfate, and ash averages over the latitude belt from the equator to 15°N where the core of the volcanic cloud resides, as a function of altitude and time in the reference experiment, FW17S111A10. The heating rates in Figure 6 are much smaller than those in Figure 3. This is because in Figure 3 heating rates are calculated for the core of a fresh cloud, but in Figure 6 they are averaged over the 0°N–15°N latitude belt. However, the comparative contributions of different heating mechanisms are invariant to the averaging over an area.

Ash absorbs SW and heats the layer above the tropopause with the average rate exceeding 1 K/day for the first 2 weeks (Figure 6a). Absorption in LW heats the volcanic cloud in the tropopause layer and in the troposphere by up to 1 K/day for the first month (Figure 6b). The interception (by ash) of upward LW flux leads to cooling of the stratosphere above the volcanic cloud up to 40 km. The total (SW + LW) ash radiative heating is significant for about 1 month, until most of the ash deposits (Figure 6c). Just after the eruption, the ash radiative effect is especially important because there is little sulfate in the volcanic cloud, with negligible heating.

The sulfate aerosol radiative effect strengthens at the beginning of July when enough SO_4 mass is formed. The lower layers of the volcanic cloud and below cool (0.02 K/day) because of the decrease of incoming SW radiation (Figure 6d). The reflected UV heats the ozone layer above the volcanic cloud (0.03 K/day). Absorption of upward LW radiation heats the cloud from below (0.3 K/day), see Figure 6e. The interception of the upward LW flux by the sulfate cloud leads to cooling of the stratosphere above the volcanic cloud. The total SW + LW heating in the stratosphere is 0.3 k/day, in agreement with Stenchikov et al. (1998), see Figure 6f.

Both ash and sulfate aerosols heat the tropopause layer. Heating by ash over the 0°N–15°N latitude belt exceeds 0.1 K/day during the first 2 weeks, which relaxes the cold point and facilitates water vapor penetration into the lower stratosphere. The heating rates caused by SO_2 are smaller in magnitude than that from sulfate aerosols both in SW and LW. In SW, SO_2 absorbs UV and heats the volcanic layer with the rate of

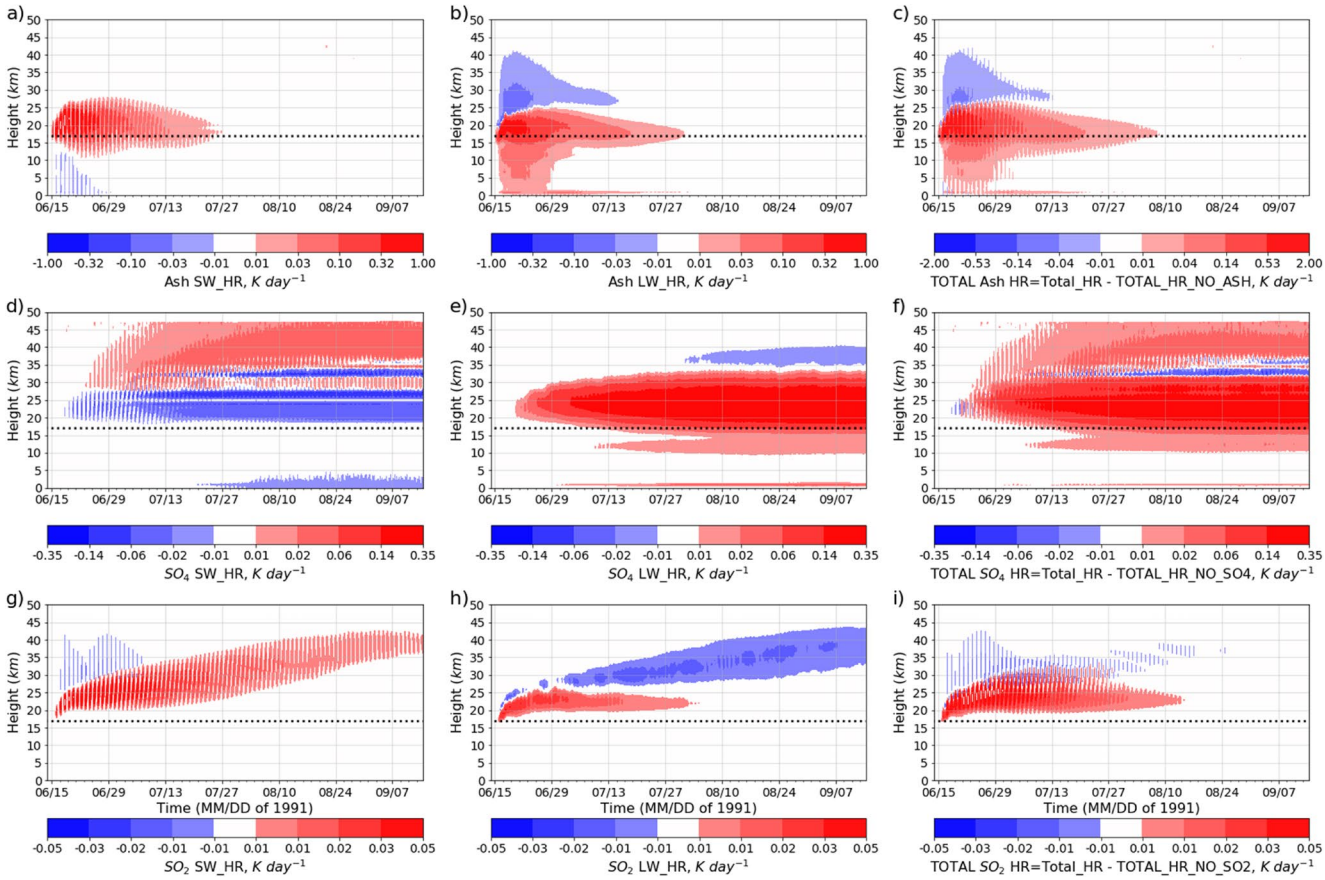

Figure 6. Daily mean radiative heating rates (K/day) averaged over the equatorial latitude belt (0°N–15°N) of ash (top row), sulfate aerosol (middle row), and SO_2 (bottom row), as a function of time and height in the reference run FW17S111A10. SW heating rates are shown in the left column, LW in the middle column, and total (SW + LW) in the right column. Dotted black line shows the 17-km injection height. LW, longwave; SW, shortwave.

5×10^{-2} K/day (Figure 6g). Because SO_2 absorbs UV photons reflected by the sulfate layer, there is a slight associated cooling of the ozone layer.

In LW, SO_2 competes with water vapor in the 16–23 μm and 7–7.5 μm wavelength bands, and with O_3 in the 8–9.6 μm wavelength bands (Zhong et al., 1996). Therefore, SO_2 radiative effect depends on the position of the SO_2 layer relative to the ozone layer. The concentration of ozone depends on height, as does the radiative effect of SO_2. The LW heating rates are of the same magnitude as the SW heating rates (Figure 6h). They are positive when the cloud is below the ozone layer in the first month after the eruption, and become negative (−0.01 K/day) from the middle of July when the cloud rises, and the layer of ozone below the cloud is thick enough to absorb upward LW flux in the narrow bands near 20 and 7.25 μm. The total (SW + LW) heating (0.05 K/day) by SO_2 was seen up to the end of July 1991. In August and September, SO_2 SW heating and LW cooling cancel each other (Figure 6i). LW, longwave; SW, shortwave.

4.4. Sensitivity of Volcanic Cloud Evolution to Input Parameters and Model Spatial Resolution

In the first week after the eruption, the volcanic cloud experiences radiative heating of 10–20 K/day (see Figure 3) and rises with an average speed of 1 km/day consistent with Equation 1. The rate of ascent depends on initial concentrations of SO_2 and ash, which depend on the volume allocated for emissions in the model. Other influential parameters are spatial resolution, the rate of gravitational settling of sulfate aerosols, its size distribution, ash radiative heating, and injection height. In this section, we quantify all those sensitivities. Figure 7a shows that volcanic cloud lofting height in the run with the sulfate aerosol size distribution B (FW17S111B10) is practically the same as in the reference experiment, while SAOD decreases

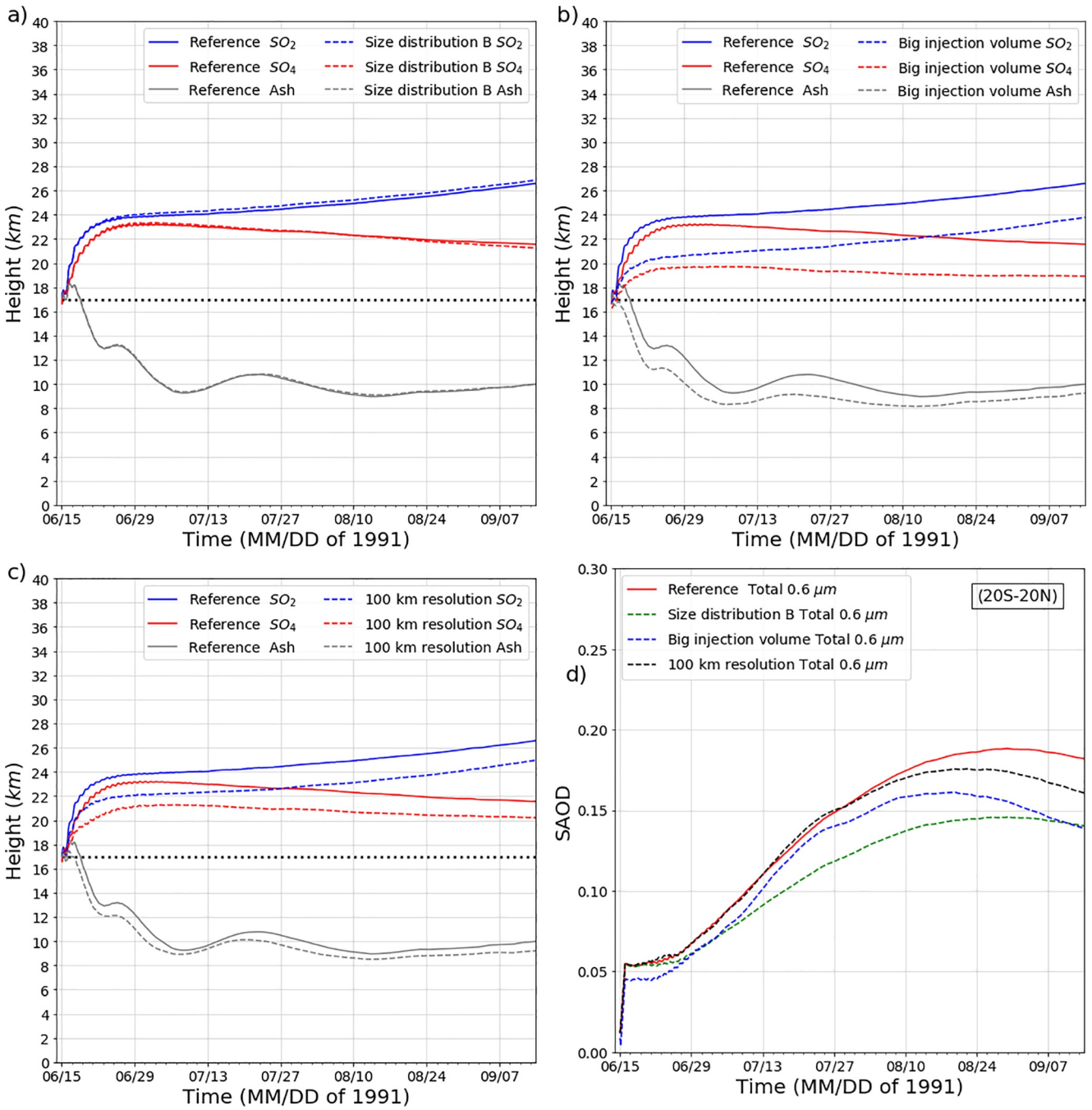

Figure 7. (a) The heights (km) of the center of mass of SO_2, SO_4, and ash clouds, as a function of time, in the reference run FW17S111A10 (solid lines) with sulfate aerosol size distribution A, and in the FW17S111B10 run (dashed lines) with sulfate aerosols size distribution (b). (b) Same as (a) but for simulation with large emission volume FW17L111A10 (dashed lines). (c) Same as (a) but for simulation with 100-km grid spacing CW17S111A10 (dashed line). (d) Total (ash + sulfate aerosols) SAOD at 0.6 μm averaged over the 20°S–20°N latitude belt in FW17S111A10 (solid red line), FW17S111B10 (dashed green), FW17L111A10 (dashed blue), and CW17S111A10 (dashed gray). Dotted black line shows the 17-km injection height. SAOD, stratospheric aerosol optical depth.

by 20% compared with the reference experiment in August-September 1991 (see Figure 7d). In the run with 100-km grid spacing, the height of the SO_2 and SO_4 clouds is about 2 km lower than in the reference run, while SAOD differs less than 15% (Figures 7c and 7d). Cloud height and SAOD are also sensitive to allocated emission volume. The height of both SO_2 and SO_4 clouds is 2–2.5 km lower in the run with a large emission volume than in the reference run. SAOD is 25% smaller in August-September 1991 and decays faster than in the reference run (Figures 7b and 7d).

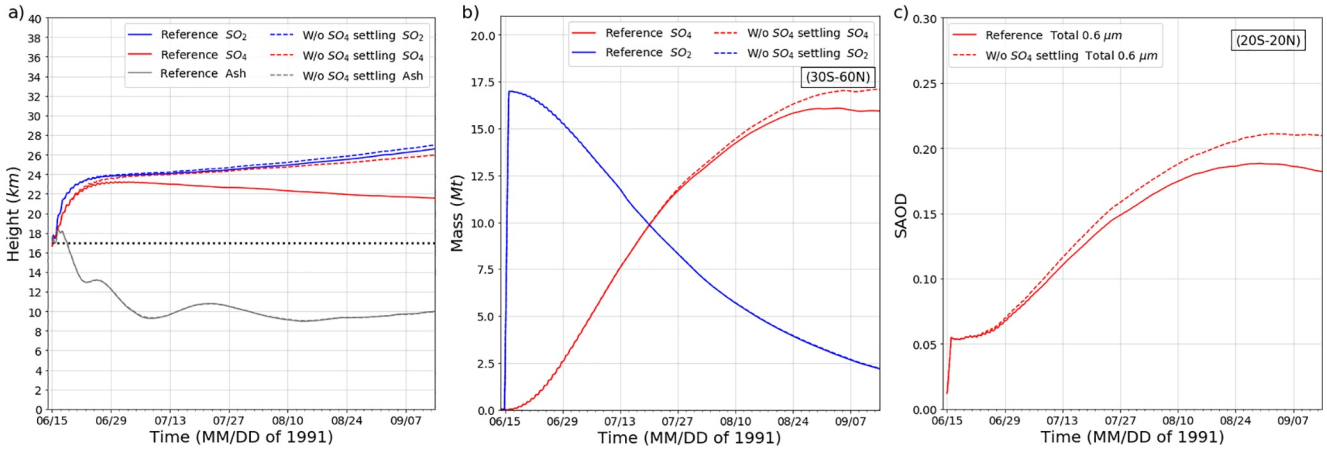

Figure 8. (a) The heights (km) of the center of mass of the SO_2 (blue), SO_4 (red), and ash (gray) clouds as a function of time. (b) Masses (Mt) of SO_2 and SO_4 in the 30°S–60°N latitude belt above 100 hPa as a function of time. (c) Stratospheric optical depth SAOD at 0.6 μm averaged over the 20°S–20°N latitude belt as a function of time. In all panels, solid lines correspond to the reference experiment FW17S111A10 and dashed lines to the FW17S111A00 experiment with sulfate aerosol gravitational settling turned off (see Table 1). Dotted black line shows the 17-km injection height. SAOD, stratospheric aerosol optical depth.

Particle size controls the efficiency of gravitational settling to remove aerosols from the stratosphere. Coarse ash settles down very quickly. For fine background stratospheric sulfate aerosols that loads the Junge layer in quiescent periods between volcanic eruptions, gravitational settling plays a secondary role as a removal process compared with BD advection to poles (Hamill et al., 1997) and deposition through tropopause folds in storm tracks (Gao et al., 2007). For coarser sulfate aerosols of volcanic origin, gravitational settling becomes a leading removal process that effectively restricts SAOD of the massive volcanic eruptions (Pinto et al., 1989; Timmreck et al., 2010). To evaluate the sensitivity of volcanic cloud evolution with respect to sulfate gravitational settling, we ran the experiment without the gravitational settling of sulfate particles (FW17S111A00).

Figure 8 compares the run FW17S111A00 (where sulfate aerosols gravitational settling is turned off) with the reference run FW17S111A10. Although the heights of SO_2 and ash clouds are practically the same in both simulations, the SO_4 cloud behaves differently. The sulfate cloud with zero settling velocity does not subside and rises together with the SO_2 cloud, remaining about 1 km below it. This demonstrates that gravitational settling plays an important role as a mechanism defining the altitude of a volcanic sulfate cloud. In the run without sulfate aerosol settling, the SO_4 mass and SAOD are 10%–15% larger than in the reference run, because SO_4 does not sediment.

Figure 9 compares the run without ash emission, FW17S1N1A10, with the reference run. The volcanic cloud lofting in the FW17S1N1A10 run during the first 2 weeks ceased (similar to the run without radiative feedback in Figure 5), indicating that the fast lifting of the cloud is driven by ash radiative heating. The SO_4 mass and SAOD in FW17S1N1A10 are two times smaller compared with the reference run, because in the experiment without ash, the sulfate and SO_2 clouds remain at lower altitudes and are depleted more intensively than in the reference experiment. This sensitivity would likely be less if we did not inject that close to the tropopause height.

Usually, it is assumed that no sulfate is present in the freshly emitted cloud. But Zhu et al. (2020) showed that SO_2 could be quickly oxidized on the surfaces of ash particles. Dhomse et al. (2014) assumed 0.75 Mt of SO_4 in the fresh Pinatubo volcanic cloud. Guo, Rose, et al. (2004) suggested that existing observations are consistent with the assumption that a fresh Pinatubo cloud contains about 4 Mt of sulfate. Scaling the heating rate in Figure 3b four times, we expect that emitting 4 Mt of SO_4 at the initial stage would generate almost as much radiative heating as ash does. To test this effect, we conduct a numerical experiment with initial emission of 4 Mt of sulfate (FW17S111A11). The amount of SO_2 is reduced to make sulfur emission invariant. Figure 10 shows that the average belt's initial total visible optical depth increases to 0.1, but the volcanic cloud evolution and the height of the center of mass of SO_2 and sulfate clouds, as well as SAOD, remain largely indifferent. This may be explained by the fact that the layer of sulfate aerosols above the

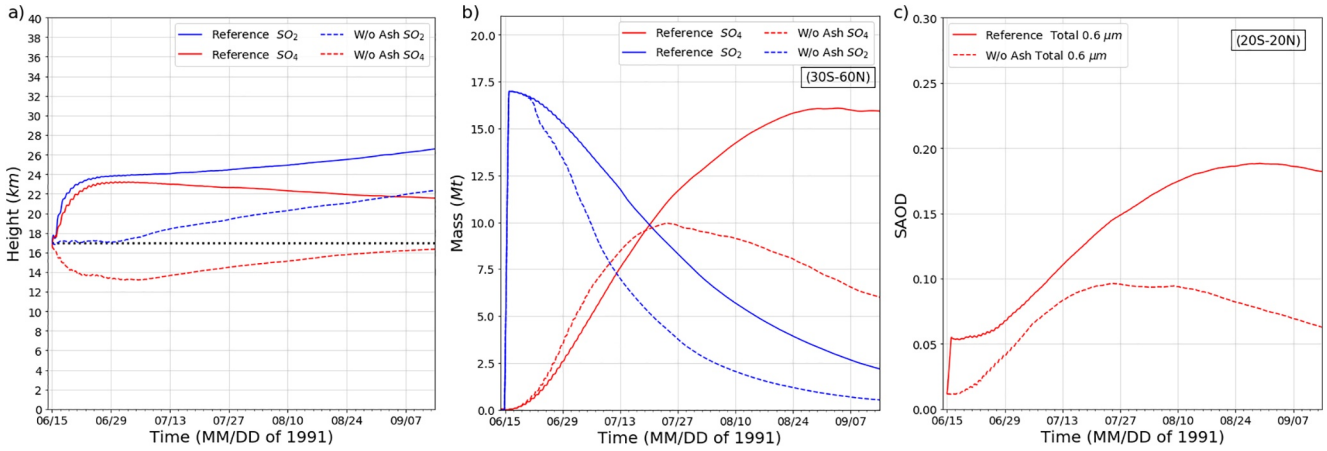

Figure 9. (a) The heights (km) of the center of mass of the SO_2 (blue) and SO_4 (red) clouds. (b) Masses (Mt) of SO_2 and SO_4 in the 30°S–60°N latitude belt above 100 hPa. (c) Total SAOD (ash + sulfate aerosols) at 0.6 μm averaged over the 20°S–20°N latitude belt. In all panels, solid lines correspond to the reference experiment FW17S111A10 and dashed lines to the experiment FW17S1N1A10 with ash emission turned off (see Table 1). Dotted black line shows the 17-km injection height. SAOD, stratospheric aerosol optical depth.

ash layer reflects SW radiation and decreases the ash radiative heating. This compensation diminishes the volcanic cloud's sensitivity to the increase of SAOD due to SO_4 initial emission.

4.5. Effect of Emission Height

Many GCM simulations of the Pinatubo event inject most of the SO_2 mass at a height of 25 km. This is a realistic assumption, since the volcanic cloud stabilizes near this level eventually, as for example, SAGE observations show (Kremser et al., 2016; Thomason, 1992; Thomason & Peter, 2006; Thomason et al., 2018). However, the initial vertical evolution of the volcanic cloud and the height of injection remain obscure, since SAGE failed to observe the volcanic cloud during the first weeks after the eruption (Thomason, 1992). So the initial dynamically active adjustment stage was largely missed from observations. As mentioned above, the way in which the volcanic cloud reaches its quasi-stationary height matters. Air density is a strong function of altitude, and the same injection mass will result in higher mixing ratios of SO_2 and ash at higher altitudes. The rate of chemical reactions depends on temperature, which is also a function of height. The SO_2 oxidation rate is sensitive to stratospheric water vapor and ozone mixing ratios, as they control the OH production, which adds in altitude sensitivity (Bekki, 1995; Bekki et al., 1996, 1993; Osipov et al., 2020).

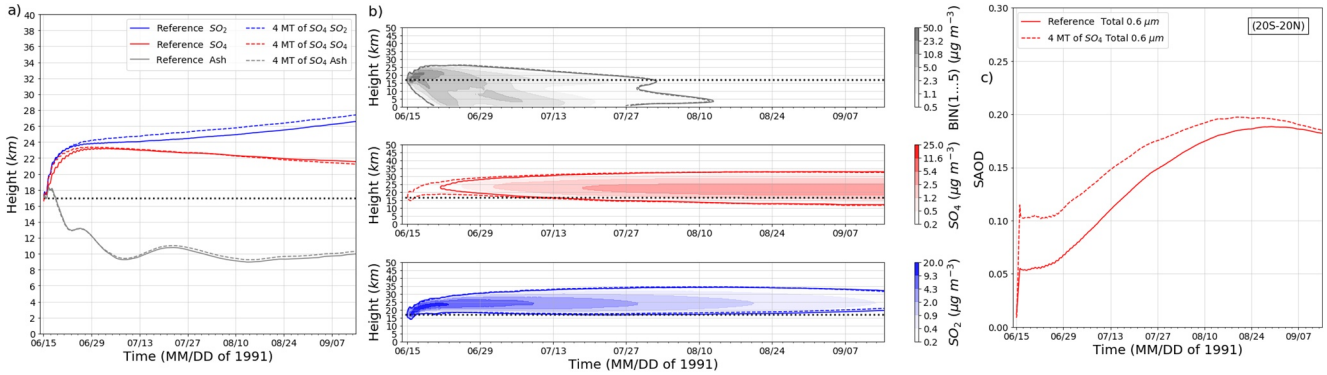

Figure 10. (a) The heights (km) of the center of mass of the SO_2 (blue), SO_4 (red), and ash (gray) clouds in the reference run FW17S111A10 (solid lines) and in the FW17S111A11 run (dashed line) with the initial release of 4 Mt of SO_4, so that the total mass of the sulfur S release remains the same (8.5 Mt) as in the reference experiment. (b) Hovmöller diagrams of SO_2, SO_4, and ash concentrations (mg/m^3), averaged over the 30°S–60°N latitude belt in the FW17S111A10 (solid lines) and FW17S111A11 (dashed line) experiments. (c) Total (ash + sulfate aerosols) SAOD at 0.6 μm averaged over the 20°S–20°N latitude belt in the FW17S111A10 (solid lines), and FW17S111A11 (dashed line) runs (see Table 1). Dotted black line shows the 17-km injection height. SAOD, stratospheric aerosol optical depth.

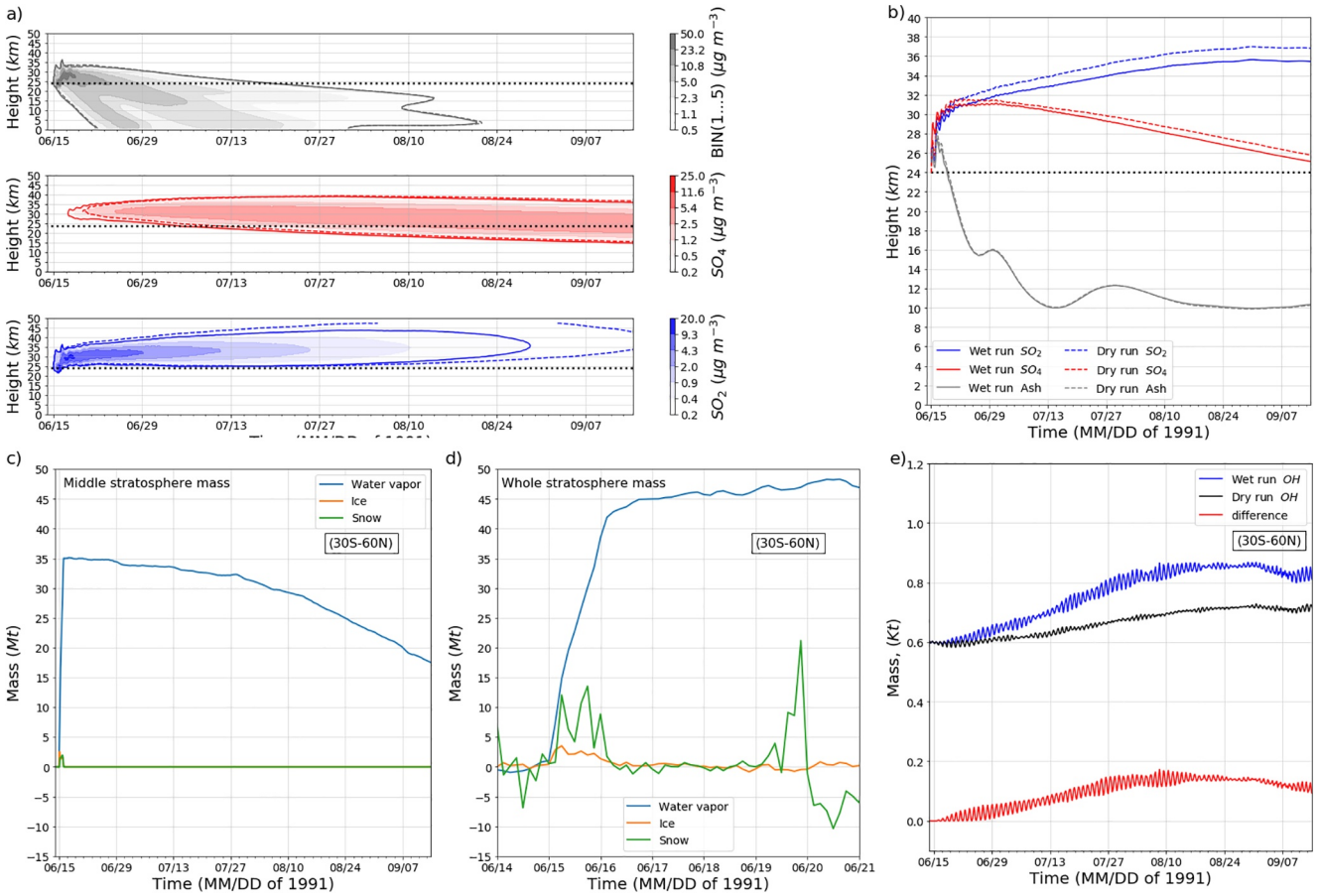

Figure 11. (a) Concentrations (μg /m^3) of SO_2 (blue), SO_4 (red), and ash (gray) averaged over the 30°S–60°N latitude belt as a function of time and height in the wet (FW24S111A10, solid lines) and the dry (FD24S111A10, dashed lines) experiments, with the emission of volcanic products at 24-km height. (b) The heights (km) of the center of mass of SO_2 (blue), SO_4 (red), and ash (gray) clouds as a function of time in the FW24S111A10 (solid lines) and FD24S111A10 (dashed lines) experiments. (c) The anomaly of the mass (Mt) of stratospheric water vapor and hydrometeors in FW24S111A10 with respect to the control run FDNNN000N00, in the middle stratosphere above 50 hPa integrated over the 30°S–60°N latitude belt, as a function of time. (d) Same as in (c), but shown for the first 6 days in the whole stratosphere above 100 hPa. (e) Masses (Kt) of OH the whole stratosphere above 100 hPa integrated over the 30°S–60°N latitude belt, as a function of time in the FW24S111A10 (blue) and FD24S111A10 (black) runs, and their difference (red). Dotted black line shows the 24-km injection height.

To quantify these sensitivities, we conducted wet (FW24S111A10) and dry (FD24S111A10) simulations, assuming volcanic injection at 24 km height (see Table 1). We did not study the sensitivity to water injections for the 17-km injection runs, as all water condenses anyway when emitted at the cold point. We also further compare the zonal average SAODs produced by 17 and 24 km injections with observations to test which one of them more closely resembles the observed SAOD.

Figure 11a shows the evolution of the ash, SO_2, and SO_4 concentrations in the FW24S111A10 (wet) and FD24S111A10 (dry) runs. The masses of emissions are the same as in the reference experiment (FW17S111A10) but the air density at 24 km is half that at 17 km. Therefore, heating rates approximately double in comparison with the reference run. The buoyancy force does not change, though, because it is proportional to the product of air density and temperature anomaly. Still, the lifting during the first 2 weeks is more vigorous than in FW17S111A10. We see sporadic increases in height due to daytime solar heating-induced instabilities. In a week, the center of mass of SO_2 and SO_4 clouds loft to the height of 32 km (Figures 11b).

Figures 11c and 11d show the anomaly of stratospheric water mass in the FW24S111A10 run with respect to the control experiment FDNN000N00, as a function of time. The stratosphere (above 100 hPa) retains 45 Mt of water vapor out of 100 Mt injected during the eruptive activity (Figures 11d). In contrast with the 17-km injection case, when the mass of water vapor above 100 hPa increases in the course of direct volcanic injection on June 15, 1991, there is no significant increase of the stratospheric water mass during the first

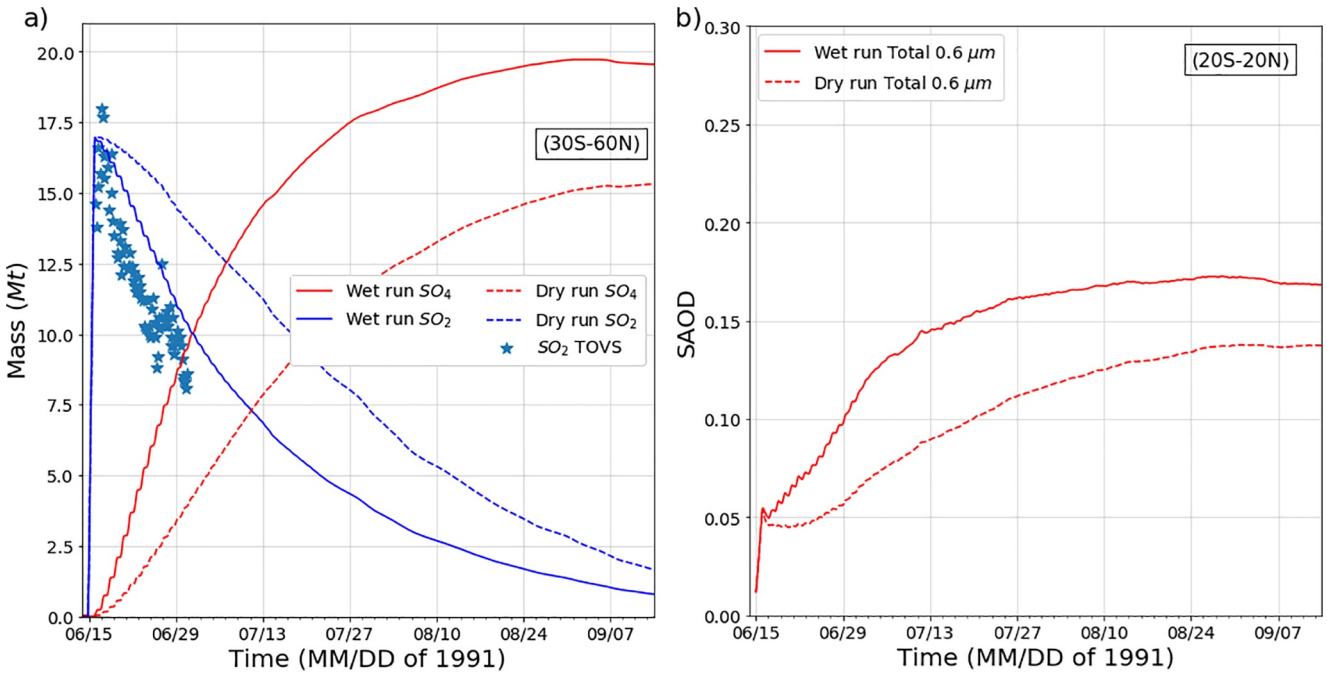

Figure 12. (a) Masses (Mt) of SO_2 (blue) and SO_4 (red) integrated over the 30°S–60°N latitude belt, as a function of time and height in the FW24S111A10 (solid lines) and FD24S111A10 (dashed lines) runs. (b) Total (ash + sulfate aerosols) SAOD averaged over the 20°S–20°N latitude belt at 0.6 μm, as a function of time in the wet FW24S111A10 (solid lines) and dry FD24S111A10 (dashed lines) runs.

week after the eruption because when volcanic products are released at 24 km, there is little heating of the tropopause layer. Up to 10 Mt of hydrometeors (ice and snow) are seen only on the first 2 days (Figures 11d), disappearing almost completely later on. The snow mass spikes on June 19–20, 1991 are not of volcanic origin, but are caused by variation of the tropopause height. Nearly all volcanic water vapor (35 Mt) resides in the middle stratosphere above 50 hPa (Figures 11c). In 3 months, the water vapor mass in the middle stratosphere decreases by about 20 Mt, close to the amount required for SO_2 to SO_4 oxidation and formation of sulfate aerosol droplets. Figure 12a shows that SO_2 to SO_4 conversion is almost 30% faster in the case with the injected water, and SAOD is significantly smaller in the dry run than in the wet run (Figure 12b). The inhibition of SO_2 oxidation in the dry run is explained by OH depletion by about 15% in the dry run compared to the wet run (Figures 11e).

Figure 13 compares the observed (SAGE/ASAP) and simulated zonal mean 1.02 μm SAODs. The SAOD structure in the reference run is close to that observed by SAGE, including the position of maximum SAOD, latitudinal spread, and duration. A significant amount of sulfate moves to the Southern hemisphere reaching 20°S, but the maximum SAOD remains in the Northern Hemisphere. In the FW24S111A10 simulation (wet 24-km injection), the sulfate aerosol SAOD develops almost two times as fast than in the reference run, but has a spatial-temporal structure which is inconsistent with observations (Figure 13d). The additional injection of 4 Mt of SO_4 (FW17S111A11, Figure 13c) leads to an increase of SAOD during the first 2 weeks of volcanic cloud evolution, but does not significantly alter the overall spatial-temporal properties of SAOD (Figure 13b).

Figure 14 shows the simulated total, sulfate aerosol, and ash SAODs at 0.6 μm in the reference run (FW17S111A10), as well as total SAOD at 0.63 μm from AVHRR observations. The AVHRR SAOD develops quicker than SAGE/ASAP SAOD in Figure 13 and is significantly bigger. But its magnitude suffers from uncertainty imposed by the removal of tropospheric background that for the considered period could be estimated only approximately. The simulated total and sulfate SAODs peak at 0.3 consistent with the previous studies (Stenchikov et al., 1998). The radiative effect of sulfate aerosols is significant from the beginning of July. Ash dominates the SAOD during the first 2 weeks, peaks at 0.73, and diminishes to 0.05 by the beginning of July. The fine ash from the first three bins in our simulations persists in the stratosphere for almost

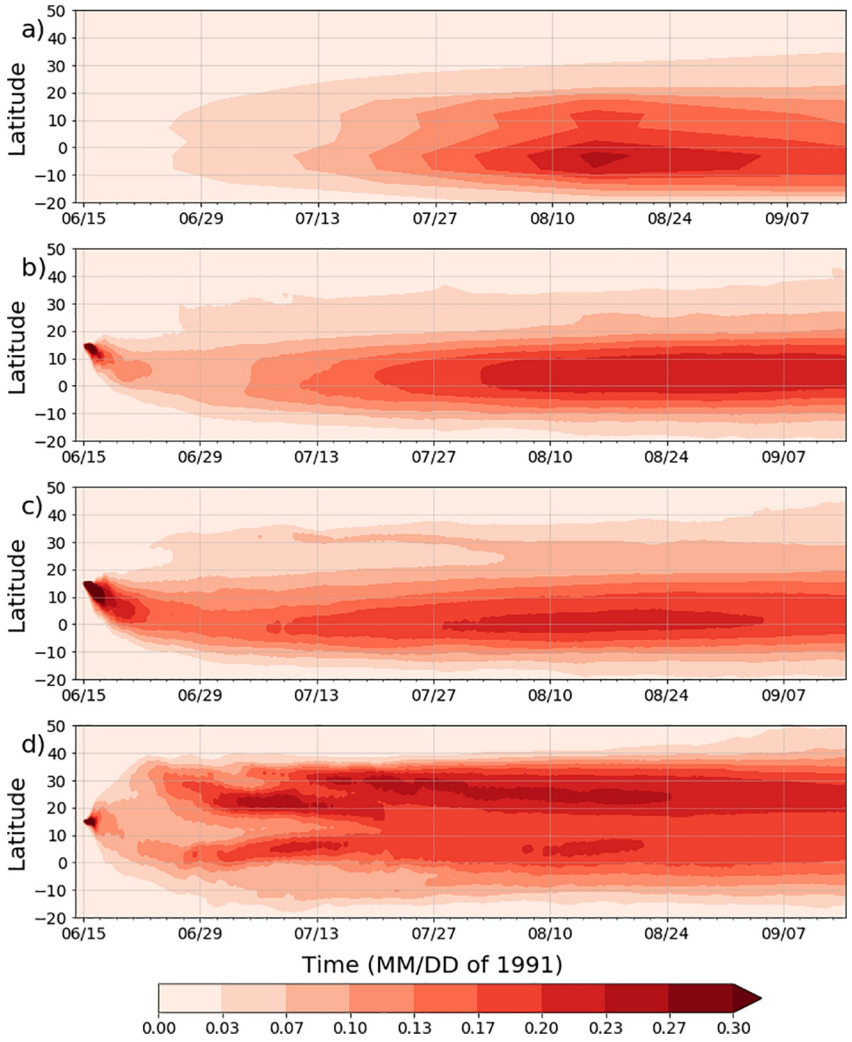

Figure 13. Hovmöller diagram of the zonal average total near IR (ash + sulfate aerosols) SAOD, as a function of time. (a) Observed by SAGE at 1.020 μm (Thomason & Peter, 2006). (b) Simulated at 1.0 μm in reference run FW17S111A10. (c) Simulated at 1.0 μm in run FW17S111A11 with the initial 4 Mt SO_4 release. (d) Simulated at 1.0 μm in the FW24S111A10 run, when volcanic products are released at the 24-km height. SAGE, Stratospheric Aerosol and Gas Experiment.

3 months (Figure 4d). This is consistent with Vernier et al. (2016) and Zhu et al. (2020), who observed fine ash in the volcanic cloud created by the Kelut eruption in 2014 for 3 months. But ash's optical depth in our runs is low in comparison with sulfate aerosols' SAOD except the first week after the eruption.

Shading in Figure 1 shows the accumulated ash deposition in the reference (FW17S111A10) run. We simulate only fine ash with $r < 10$ μm emitting it at the height of the injection (17 km), and do not capture the deposition over the South China Sea. We see strong deposition spots over the Indian ocean and Africa in the Intertropical Convergence Zone (ITCZ).

For completeness we also performed a run with volcanic materials erupted at an intermediate height of 20.5 km. Figure 15 shows the comparison of the numerical experiment with the 20.5-km injection height (FW20S111A10) and the reference experiment (FW17S111A10). The 20.5-km injection experiment shows practically the same SAOD, shifted up by 2–3 km volcanic cloud trajectories, and incorrect spatial temporal structure of the zonal mean SAOD.

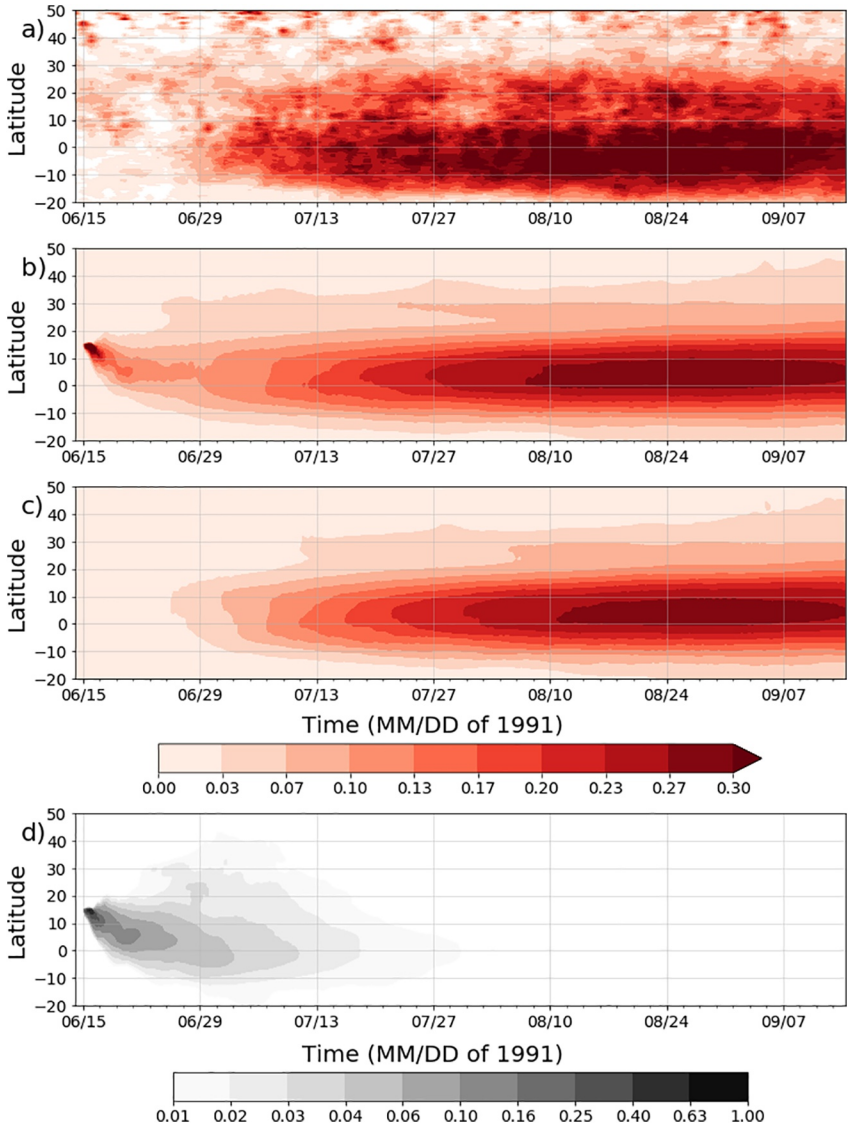

Figure 14. Hovmöller diagram of zonal mean SAOD: (a) observed by AVHRR at 0.63 μm and simulated at 0.6 μm in reference run FW17S111A10, (b) total (ash + sulfate aerosols) SAOD, (c) Sulfate aerosols SAOD, peaking at 0.3, (d) ash SAOD, peaking at 0.73. AVHRR, Advanced Very High-Resolution Radiometer; SAGE, Stratospheric Aerosol and Gas Experiment.

4.6. Sensitivity to Injected Masses of Eruptive Products

The injected masses of SO_2, ash, and water vapor indeed matter for the evolution of a volcanic cloud. The sensitivity to SO_2 injected mass is well known. This sensitivity complicates by the nonlinear effect of aerosol microphysics (Clyne et al., 2020). Guo, Bluth, et al. (2004) ranged the Pinatubo SO_2 emission mass from 14 to 20 Mt so that 17 Mt is in the middle of this range. The most recent observational SO_2 mass estimate (Fisher et al., 2019) puts the lower limit at 12 Mt instead of 14 Mt. The 17 Mt SO_2 mass works well in our simulations as it produces the sulfate aerosol optical depth consistent with observations for the simulated period (see Figure 4). One cannot arbitrarily change SO_2 mass in the same model without breaking consistency between simulated and observed SAOD. WACCM (Mills et al., 2016) estimates the lowest SO_2 emission because it predicts too small aerosol particles that produce more considerable optical depth per unit mass. In our model, we must use 17 Mt of SO_2 to fit observations. This discrepancy between the models is consistent with the VolMIP conclusion (Clyne et al., 2020) that there are significant model uncertainties in the calculations of aerosol microphysics and chemistry. Our simulations are less affected by this problem

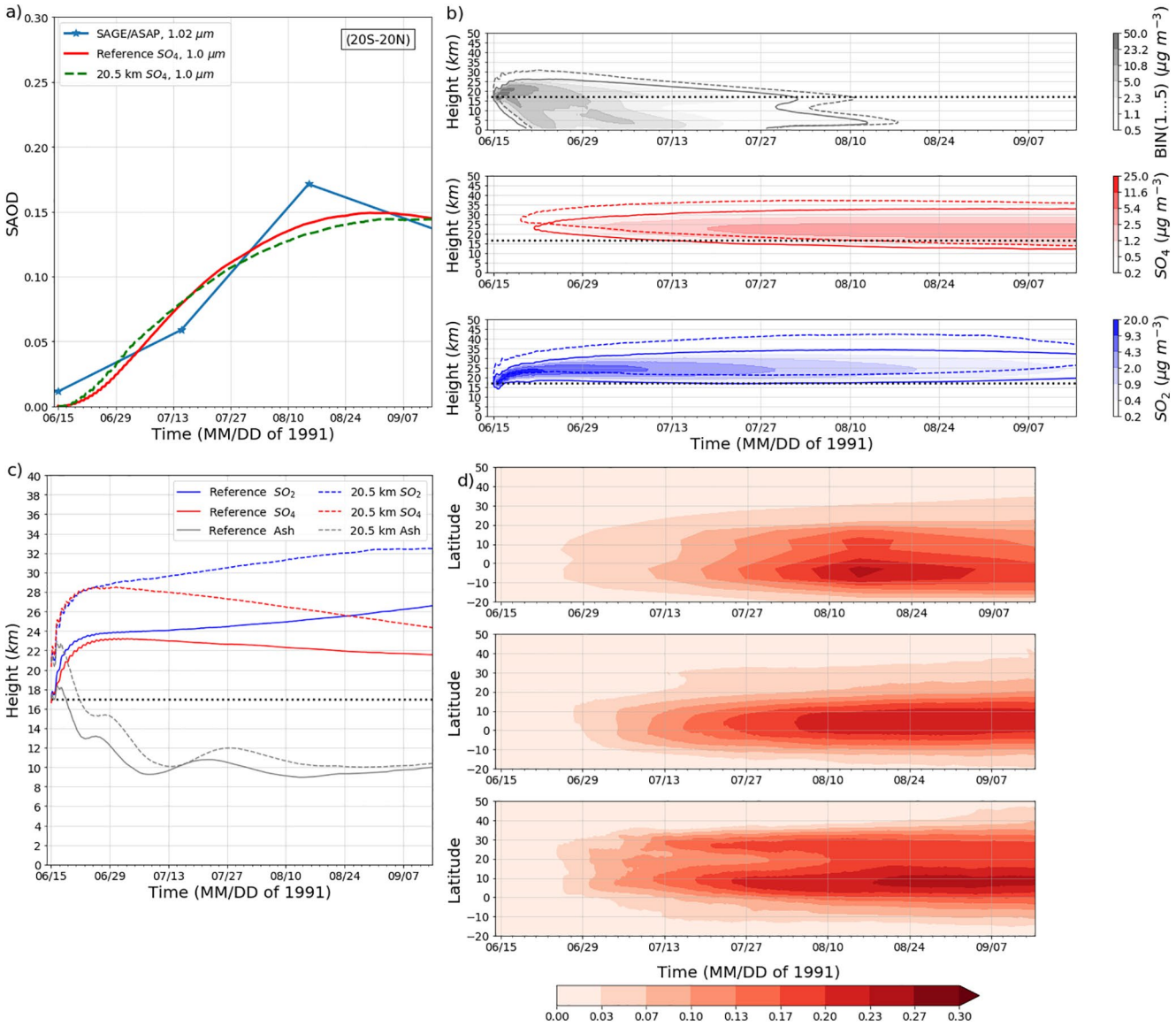

Figure 15. The comparison of the numerical experiment with the 20.5-km injection height (FW20S111A10) with the reference experiment (FW17S111A10). Dotted black line shows the 17-km injection height. (a) Simulated sulfate aerosol SAOD at 1.0 μm averaged over the 20°S–20°N latitude belt, as a function of time for reference experiment (solid red) and the experiment with 20.5-km injection height. The observed SAGE/ASAP at 1.02 μm (Thomason & Peter, 2006) 20°S–20°N mean SAODs are shown by blue lines with markers. The model diagnostics are averaged over the same overlapping areas where SAGE/ASAP data are available. (b) Hovmöller diagrams of ash (gray), SO_4 (red), and SO_2 (blue) and concentrations (μg /m^3) averaged over the 30°S–60°N latitude belt as a function of time and height in FW20S111A10 run. Dashed contour lines correspond to the FW20S111A10 run with the 20.5 injection height. Solid lines correspond to the FW17S111A10 reference run. (c) The heights (km) of the center of mass of SO_4 (red), SO_2 (blue), and ash (gray) clouds. Dashed contour lines correspond to the FW20S111A10 run with the 20.5 injection height. Solid lines correspond to the FW17S111A10 reference run. (d) Hovmöller diagram of the zonal average total near IR sulfate aerosol SAOD, as a function of time. Top: Observed by SAGE/ASAP at 1.020 μm (Thomason & Peter, 2006). Middle: Simulated at 1.0 μm in reference run FW17S111A10. Bottom: Simulated at 1.0 μm in run FW20S111A11 with the injection height of 20.5 km. SAGE, Stratospheric Aerosol and Gas Experiment; SAOD, stratospheric aerosol optical depth.

than the state-of-the-art global models because we use the simplified sulfate aerosol microphysics with prescribed (from observations) aerosol size distribution. This directly links SAOD and SO_2 mass so that the observed SAOD constrains the SO_2 mass.

The heterogeneous reactions on ash surfaces uncovered in Zhu et al. (2020) are undoubtedly an important new finding that affects SO_2 mass estimates. But SO_2 uptake on aerosol surfaces happens quickly, so that the satellite measurements of SO_2 mass for a few days after an eruption should account for this effect. For

the Pinatubo, the satellite measurements even show an increase in SO_2 mass (Fisher et al., 2019; Guo, Bluth, et al., 2004) a few days after the eruption.

Extra "volcanic" water affects both radiative heatings of a volcanic cloud and accelerates SO_2 oxidation by increasing concentration of OH radicals. But the temperature at the injection height completely controls the water vapor mass retained in the stratosphere, so that it almost does not matter how much water we initially release as soon as the emitted mass is above the limit that could be retained in the stratosphere at the chosen emission height.

Ash makes a major impact on cloud lofting. However, its effect is controlled not as much by its total mass but by its size distribution. To test this we conducted a sensitivity experiment where we removed emission in the coarse ash bin(5) reducing the total ash mass almost by half. Figure 16 shows the comparison of the numerical experiment FW17S121A10 with omitted coarse ash Bin (5) and the reference experiment FW-17S111A10. The experiment FW17S121A10 with almost halved mass of emitted ash differs very little from the reference run.

To further test the sensitivity to the amount of emitted ash we conducted the numerical experiment halving the mass in all ash bins (FW17S131A10) in comparison with the whole physics reference run (FW-17S111A10), see Table 1. Figure 17 compares results from FW17S131A10 and FW17S111A10. The sulfate cloud optical depth (Figure 17a) practically does not change in comparison with the reference experiment The total mass of ash (Figure 17b) is 37.5 Mt, less than in the very moderate estimate of Gouhier et al. (2019), but lofting of aerosol remains significant. The heights of the center of mass of SO_2 and SO_4 clouds are only 2 km lower than in the reference run. The SAOD in Figure 17d is slightly narrower in latitude in comparison with observations and FW17S111A10 run, but exhibits spatial-temporal structure of observed SAOD relatively well.

Zhu et al. (2020) considered the Kelut eruption that emitted 100 times less SO_2 than Pinatubo so that the aerosol radiative feedback in their case is negligible. In their study, a significant (compared with sulfate in terms of their radiative effect) mass of fine ash particles remains in the atmosphere for a few months interacting with SO_2 and sulfate aerosols. In the GOCART aerosol model, we use five bins to approximate the ash size distribution. The finest bin radii are in the range of $0.1 < r < 1$ μm. Particles in this bin are long-lived, but the bin is weakly populated. It is hard to argue about increasing the mass of very fine ash for the Pinatubo case because this will lead to overheating of the stratosphere by volcanic aerosols in the long-term and make the lifting of volcanic debris unrealistically vigorous in the short-term. This is consistent with the Gouhier et al. (2019) finding that volcanic clouds from large Plinian eruptions contains two orders of magnitude smaller fraction of fine ash than moderate and weak explosions. The "radiative feedback" restriction on the amount of fine ash is not seen on eruptions two orders of magnitude weaker than Pinatubo, like Kelut, because radiative feedback for small eruptions is negligible both for sulfate aerosol and for ash. But this "radiative feedback" is a strong constraint for the 1991 Pinatubo eruption that released two orders of magnitude more volcanic debris than Kelut.

5. Conclusions

We have improved the community regional meteorology-chemistry model WRF-Chem by implementing physical and chemical mechanisms that are necessary to simulate the realistic evolution of the volcanic cloud in the stratosphere and the upper troposphere. We employed the new capabilities of WRF-Chem to simulate the volcanic cloud of the 1991 Pinatubo eruption. The regional model setting allowed us to keep the meteorology realistic and support a high spatial resolution, so that we were able to quite realistically reproduce typhoon Yunay observed at the time of the eruption. The simulations were conducted with 25-km grid spacing for 3 months accounting for the right phase of QBO and simultaneously injecting water vapor, ash, SO_2, and SO_4. We have calculated vertical lifting and horizontal transport of a volcanic cloud accounting for the radiative effect of all of the tracers, SO_2, ash, water vapor, and sulfate aerosols. The sulfur cycle, differential self-lofting of sulfate, SO_2, and ash clouds, gravitational settling of ash and sulfate particles, and OH concentration, have been calculated interactively, but the ozone profile has been prescribed from observations. The spatial resolution and physical consistency we achieved in this study are superior in comparison with the previous simulations of the 1991 Mt. Pinatubo eruption.

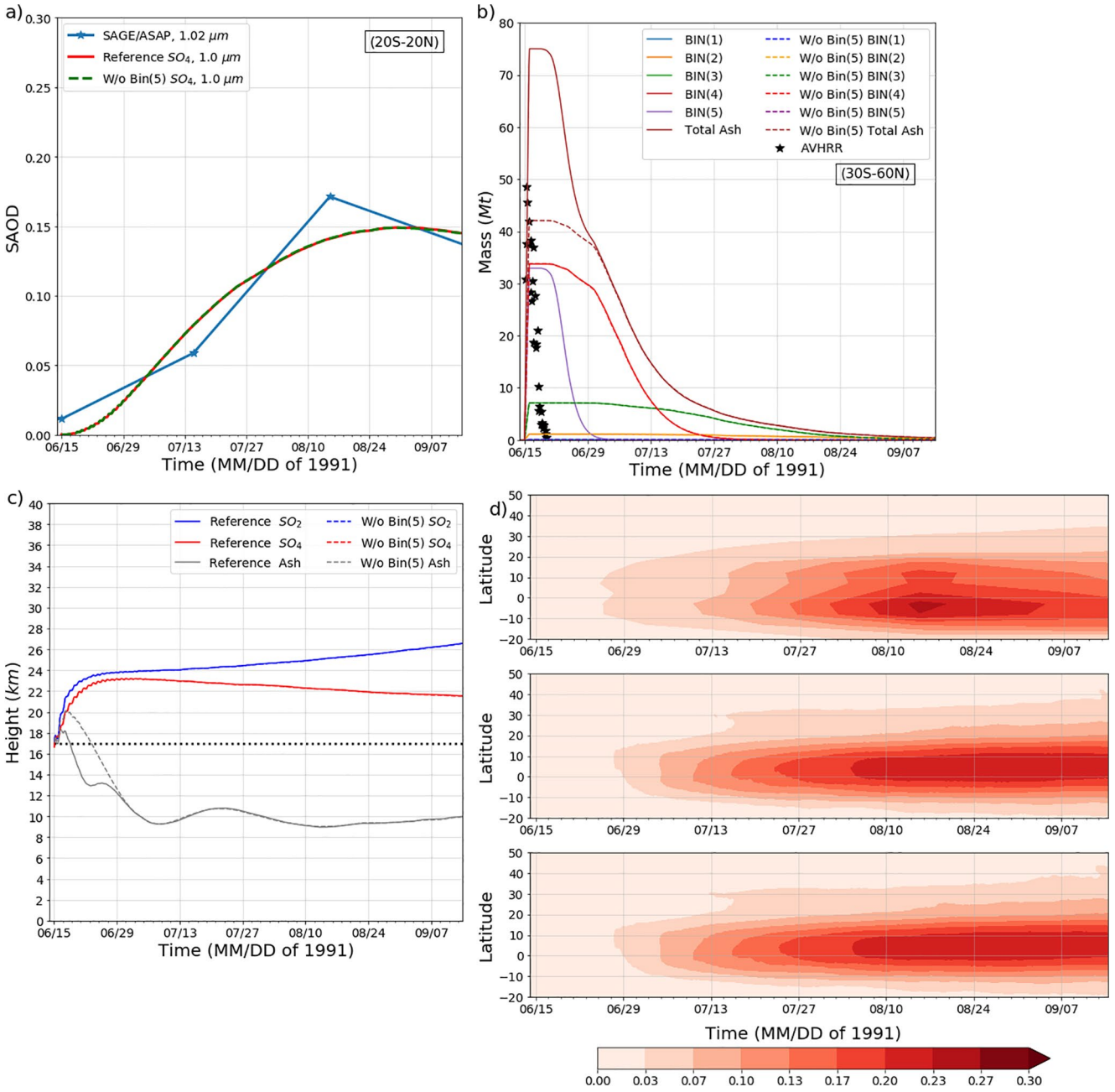

Figure 16. The comparison of the numerical experiment with omitted coarse ash bin(5) (FW17S121A10) with the reference experiment (FW17S111A10). Dotted black line shows the 17-km injection height. (a) Simulated sulfate aerosol SAOD at 1.0 μm averaged over the 20°S–20°N latitude belt, as a function of time for reference experiment (solid red) and the experiment without coarse ash bin(5) (dashed green). The observed SAGE at 1.02 μm (Thomason & Peter, 2006) 20°S–20°N mean SAODs are shown by blue lines with markers. The model diagnostics are averaged over the same overlapping areas where SAGE/ASAP data are available. (b) Masses (Mt) of ash in each of five ash bins (bin(5) is zeroed in FW17S121A10) and their total mass in FW17S121A10 and reference run FW17S111A10 integrated over the 30°S–60°N latitude belt, as a function of time. The AVHRR retrievals of the mass of fine ash (diameters 0–15 μm) are shown by markers (Guo, Rose, et al., 2004). (c) The heights (km) of the center of mass of SO_4 (red), SO_2 (blue), and ash (gray) clouds. Solid lines correspond to the FW17S111A10 reference run. Dashed lines correspond to the FW17S121A10 run. (d) Hovmöller diagram of the zonal average total near IR sulfate aerosol SAOD, as a function of time. Top: Observed by SAGE/ASAP at 1.020 μm (Thomason & Peter, 2006). Middle: Simulated at 1.0 μm in reference run FW17S111A10. Bottom: Simulated at 1.0 μm in the FW17S121A10 run without coarse ash bin(5). SAGE, Stratospheric Aerosol and Gas Experiment; SAOD, stratospheric aerosol optical depth.

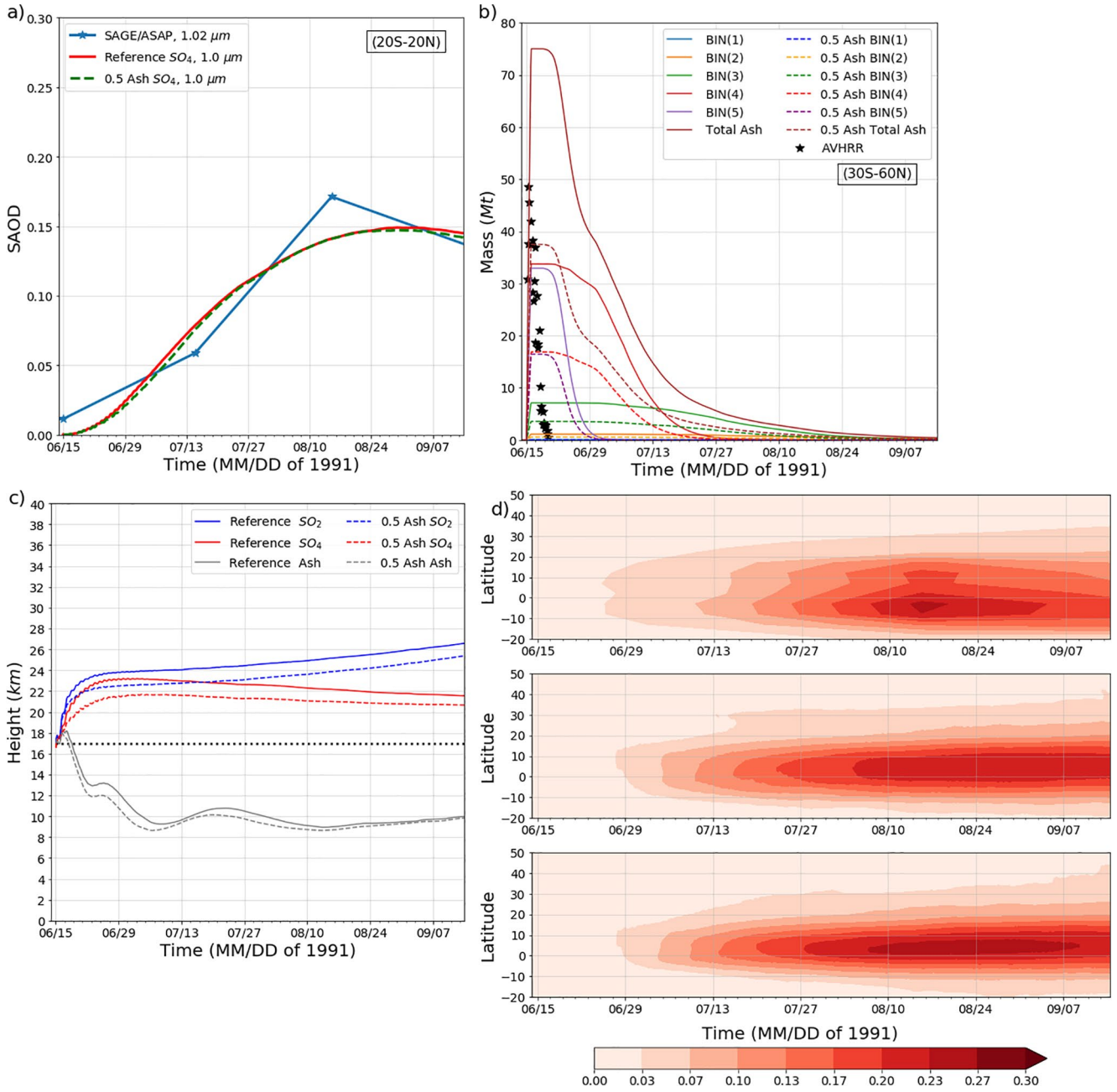

Figure 17. The comparison of the numerical experiment with halved emitted ash mass in all five bins (FW17S131A10) with the reference experiment (FW17S111A10). Dotted black line shows the 17-km injection height. (a) Simulated sulfate aerosol SAOD at 1.0 μm averaged over the 20°S–20°N latitude belt, as a function of time for reference experiment (solid red) and the experiment with halved ash mass (dashed green). The observed SAGE at 1.02 μm (Thomason & Peter, 2006) 20°S–20°N mean SAODs are shown by blue lines with markers. The model diagnostics are averaged over the same overlapping areas where SAGE/ASAP data are available. (b) Masses (Mt) of ash in each of five ash bins and their total mass in FW17S131A10 and reference run FW17S111A10 integrated over the 30°S–60°N latitude belt, as a function of time. The AVHRR retrievals of the mass of fine ash (diameters 0–15 μm) are shown by markers (Guo, Rose, et al., 2004). (c) The heights (km) of the center of mass of SO_4 (red), SO_2 (blue), and ash (gray) clouds. Solid lines correspond to the FW17S111A10 reference run. Dashed lines correspond to the FW17S131A10 run. (d) Hovmöller diagram of the zonal average total near IR sulfate aerosol SAOD, as a function of time. Top: Observed by SAGE/ASAP at 1.020 μm (Thomason & Peter, 2006). Middle: Simulated at 1.0 μm in reference run FW17S111A10. Bottom: Simulated at 1.0 μm in the FW17S131A10 run with halved ash mass. SAGE, Stratospheric Aerosol and Gas Experiment; SAOD, stratospheric aerosol optical depth.

We have studied the sensitivity of the cloud evolution to the input parameters, physical assumptions, and model resolution (see Table 1). We found that the cloud lofting velocity is sensitive to the initial concentration of eruptive products, but the model results are weakly sensitive to the assumption regarding amount of injected water vapor and ash, as well as sulfate aerosol size distribution, because lofting is driven by ash SW and LW absorption. The effect of the sulfate aerosol gravitational settling on SO_4 mass and SAOD is about 10% but deposition velocities define the level of neutral buoyancy for the SO_4 cloud. The increase in horizontal resolution from the 100-km grid spacing to 25 km leads to a 2-km increase in the cloud lofting height (about 30%) and less than 5% increase in SAOD. The initial release of 4 Mt of SO_4, which mimics the effect of the quick SO_2 oxidation on ash surfaces (Zhu et al., 2020) appears to have a minor effect on the volcanic cloud development. The large-scale dynamic variability in our settings is damped by imposing lateral boundary conditions from the reanalysis. The low sensitivity of cloud evolution to the main physical assumptions and numerical parameters indicates the robustness of the model results. The main physical findings could be formulated as follows:

- Differential radiative heating and gravitational settling lead to a separation of ash, SO_2, and sulfate clouds. The cloud evolution, and especially the effect of water, depend drastically on the initial height of the emission. In our model experiments, SO_4 and SO_2 clouds in the presence of ash have an ability to rise 7 km above the level of initial injection during the first week of evolution. See Figure 5.
- During the first week after an eruption, the cloud lofts about 1 km/day, while the BD updraft velocity is about 20 m/day. The SO_4 cloud then subsides because of the gravitational settling of sulfate particles, but the SO_2 cloud continues rising in the BD upward motion. Ash particles with radii $r > 3$ μm deposit within a month, while smaller ash particles stay in the stratosphere the entire period of simulations. See Figures 4 and 5.
- The visible optical depth of ash in the volcanic cloud peaks at about 9 just after the eruption. The radiative heating of ash within the cloud reaches 20 K/day and drives the cloud uplift during the first week. Overall, ash radiative heating is significant during the first month. The radiative effect of SO_2 is smaller than that of ash or sulfate aerosols, but remains significant during the first month. The radiative heating effect of sulfate aerosols develops in two weeks after an eruption, as soon as enough sulfate is developed. In September, the SW + LW radiative heating of the cloud reaches 0.3 K/day. In the long-term, SO_2 heating is an order of magnitude smaller than that of sulfate aerosols but maintains a permanent rise of the SO_2 cloud. See Figures 3 and 6.
- The amount of water remaining in the cloud is controlled by the height and temperature of the level where eruption products are released. Practically all water is lost to sedimentation as ice and snow if the volcanic material is released just above the tropopause. However, above-tropopause injections can warm the tropopause and increase cross-tropopause water transport into the stratosphere. A significant amount of water remains in the cloud immediately after an eruption if the volcanic material is released well above the tropopause. The radiative effect of water vapor and hydrometeors is insignificant compared with ash. Still, the presence of extra water vapor in the volcanic cloud accelerates the SO_2 conversion into sulfate by 30%, affecting the vertical distribution of SO_2 and SO_4. See Figures 4, 6, and 11.
- Ash and SO_2 effectively inhibit the UV actinic flux and O_3 photolysis in the fresh, dense cloud. This leads to an initial average over the domain decrease in OH mass by about 10%. In the wet 24-km injection experiment, OH mass subsequently increases by 30% when the ash and SO_2 UV optical depth decreases and extra volcanic water facilitates OH production. See Figures 3, 4, and 11.
- The SAOD spatial-temporal evolution in the 24-km injection run is qualitatively incompatible with observations. Conversely, a 17-km injection reference run exhibits a SAOD spatial-temporal evolution similar to observations. This suggests that most of the SO_2 mass in the 1991 Pinatubo eruption has been released at 17-km by co-ignimbrite convection and lifted in the middle stratosphere by the self-lofting mechanism. See Figures 13 and 14.
- Ash optical depth diminishes rapidly and does not produce a direct long-term climate effect, yet it plays a crucial role in the dynamical lifting of the cloud during the first week after an eruption. This initial lofting is of primary importance since it controls the mass loss from the cloud due to mixing down through the tropopause. Ash heating accounts for 50% of SO_2 and SO_4 mass in the cloud (and SAOD) during the first two months (see Figure 9). The inclusion of ash doesn't change the sulfur mass releases, it only changes the amount of that mass that remains in the stratosphere, through the lofting due to heating of the ash.

The developed regional model could be useful in multiple applications, from the impact of volcanic clouds on aviation and propagation of soot from pyro-convection into the lower stratosphere to calculating volcanic cloud's effect on climate. The radiative effect of eruption products potentially could significantly improve the model's ability to predict the transport and longevity of tropospheric and stratospheric volcanic clouds. Further improvement of microphysical processes within the volcanic cloud could be implemented using existing WRF-Chem microphysical modules, for example, Model for Simulating Aerosol Interactions and Chemistry. A more realistic description of the fine-scale dispersion of volcanic clouds could be beneficial for designing geoengineering technologies, such as those based on Solar Radiation Management, which assumes aerosol precursors' emissions into the lower stratosphere to develop an aerosol reflection layer for cooling the Earth.

Conflict of Interest

The authors declare no conflicts of interest relevant to this study.

Data Availability Statement

The ERA-Interim reanalysis data were obtained from the ECMWF Data Server with 0.75° by 0.75° horizontal and 6-h temporal resolution. The SAGE data (Thomason & Peter, 2006) were obtained from the Stratosphere-troposphere Processes, and their Role in Climate (SPARC) website (https://www.sparc-climate.org/data-centre/data-access/assessment-of-stratospheric-aerosol-properties/). The modeling framework and data necessary to reproduce the simulations are publicly available through KAUST Repository (http://hdl.handle.net/10754/664920).

Acknowledgments
The study reported in this publication was supported by funding from King Abdullah University of Science and Technology (KAUST) through Grant BAS/1/1309-01-01. The authors thank the KAUST Supercomputing Laboratory for providing computer resources.

References

Angell, J. K. (1997). Estimated impact of Agung, El Chichon and Pinatubo volcanic eruptions on global and regional total ozone after adjustment for the QBO. *Geophysical Research Letters*, *24*(6), 647–650. https://doi.org/10.1029/97gl00544

Aquila, V., Oman, L. D., Stolarski, R. S., Colarco, P. R., & Newman, P. A. (2012). Dispersion of the volcanic sulfate cloud from a Mount Pinatubo-like eruption. *Journal of Geophysical Research: Atmospheres*, *117*(D6). https://doi.org/10.1029/2011jd016968

Aubry, T. J., Jellinek, A. M., Degruyter, W., Bonadonna, C., Radić, V., Clyne, M., & Quainoo, A. (2016). Impact of global warming on the rise of volcanic plumes and implications for future volcanic aerosol forcing. *Journal of Geophysical Research: Atmospheres*, *121*(22). 13326–13351. https://doi.org/10.1002/2016jd025405

Bardeen, C. G., Toon, O. B., Jensen, E. J., Marsh, D. R., & Harvey, V. L. (2008). Numerical simulations of the three-dimensional distribution of meteoric dust in the mesosphere and upper stratosphere. *Journal of Geophysical Research*, *113*(D17). https://doi.org/10.1029/2007jd009515

Bekki, S. (1995). Oxidation of volcanic SO_2: A sink for stratospheric OH and H_2O. *Geophysical Research Letters*, *22*(8), 913–916. https://doi.org/10.1029/95gl00534

Bekki, S., & Pyle, J. A. (1994). A two-dimensional modeling study of the volcanic eruption of Mount Pinatubo. *Journal of Geophysical Research*, *99*(D9), 18861–18869. https://doi.org/10.1029/94jd00667

Bekki, S., Pyle, J. A., Zhong, W., Toumi, R., Haigh, J. D., & Pyle, D. M. (1996). The role of microphysical and chemical processes in prolonging the climate forcing of the Toba Eruption. *Geophysical Research Letters*, *23*(19), 2669–2672. https://doi.org/10.1029/96gl02088

Bekki, S., Toumi, R., & Pyle, J. A. (1993). Role of sulphur photochemistry in tropical ozone changes after the eruption of Mount Pinatubo. *Nature*, *362*(6418), 331–333. https://doi.org/10.1038/362331a0

Bluth, G. J. S., Doiron, S. D., Schnetzler, C. C., Krueger, A. J., & Walter, L. S. (1992). Global tracking of the SO_2 clouds from the June, 1991 Mount Pinatubo eruptions. *Geophysical Research Letters*, *19*(2), 151–154. https://doi.org/10.1029/91gl02792

Bluth, G. J. S., Schnetzler, C. C., Krueger, A. J., & Walter, L. S. (1993). The contribution of explosive volcanism to global atmospheric sulphur dioxide concentrations. *Nature*, *366*(6453), 327–329. https://doi.org/10.1038/366327a0

Borrmann, S., Dye, J. E., Baumgardner, D., Proffitt, M. H., Margitan, J. J., Wilson, J. C., et al. (1995). Aerosols as dynamical tracers in the lower stratosphere: Ozone versus aerosol correlation after the Mount Pinatubo eruption. *Journal of Geophysical Research*, *100*(D6), 11147–11156. https://doi.org/10.1029/95jd00016

Brock, C. A., Hamill, P., Wilson, J. C., Jonsson, H. H., & Chan, K. R. (1995). Particle formation in the upper tropical troposphere: A source of nuclei for the stratospheric aerosol. *Science*, *270*(5242), 1650–1653. https://doi.org/10.1126/science.270.5242.1650

Brühl, C., Lelieveld, J., Crutzen, P. J., & Tost, H. (2012). The role of carbonyl sulphide as a source of stratospheric sulphate aerosol and its impact on climate. *Atmospheric Chemistry and Physics*, *12*(3), 1239–1253. https://doi.org/10.5194/acp-12-1239-2012

Brühl, C., Lelieveld, J., Tost, H., Höpfner, M., & Glatthor, N. (2015). Stratospheric sulfur and its implications for radiative forcing simulated by the chemistry climate model EMAC. *Journal of Geophysical Research: Atmospheres*, *120*(5), 2103–2118. https://doi.org/10.1002/2014jd022430

Brühl, C., Schallock, J., Klingmüller, K., Robert, C., Bingen, C., Clarisse, L., et al. (2018). Stratospheric aerosol radiative forcing simulated by the chemistry climate model EMAC using Aerosol CCI satellite data. *Atmospheric Chemistry and Physics*, *18*(17), 12845–12857. https://doi.org/10.5194/acp-18-12845-2018

Caldeira, K., Bala, G., & Cao, L. (2013). The science of geoengineering. *Annual Review of Earth and Planetary Sciences*, *41*(1), 231–256. https://doi.org/10.1146/annurev-earth-042711-105548

Carn, S. A., Clarisse, L., & Prata, A. J. (2016). Multi-decadal satellite measurements of global volcanic degassing. *Journal of Volcanology and Geothermal Research*, *311*, 99–134. https://doi.org/10.1016/j.jvolgeores.2016.01.002

Chin, M., Diehl, T., Dubovik, O., Eck, T. F., Holben, B. N., Sinyuk, A., & Streets, D. G. (2009). Light absorption by pollution, dust, and biomass burning aerosols: A global model study and evaluation with AERONET measurements. *Annales Geophysicae*, *27*(9), 3439–3464. https://doi.org/10.5194/angeo-27-3439-2009

Chin, M., Diehl, T., Tan, Q., Prospero, J. M., Kahn, R. A., Remer, L. A., et al. (2014). Multi-decadal aerosol variations from 1980 to 2009: A perspective from observations and a global model. *Atmospheric Chemistry and Physics*, *14*(7), 3657–3690. https://doi.org/10.5194/acp-14-3657-2014

Chin, M., Ginoux, P., Kinne, S., Torres, O., Holben, B. N., Duncan, B. N., et al. (2002). Tropospheric aerosol optical thickness from the GOCART model and comparisons with satellite and Sun photometer measurements. *Journal of the Atmospheric Sciences*, *59*(3), 461–483. https://doi.org/10.1175/1520-0469(2002)059<0461:TAOTFT>2.0.CO;2

Clyne, M., Lamarque, J. F., Mills, M. J., Khodri, M., Ball, W., Bekki, S., et al. (2020). Model physics and chemistry causing intermodel disagreement within the VolMIP-Tambora interactive stratospheric aerosol ensemble. *Atmospheric Chemistry and Physics*, 1–43.

Considine, D. B., Rosenfield, J. E., & Fleming, E. L. (2001). An interactive model study of the influence of the Mount Pinatubo aerosol on stratospheric methane and water trends. *Journal of Geophysical Research*, *106*(D21), 27711–27727. https://doi.org/10.1029/2001jd000331

Costa, A., Suzuki, Y. J., Cerminara, M., Devenish, B. J., Ongaro, T. E., Herzog, M., et al. (2016). Results of the eruptive column model inter-comparison study. *Journal of Volcanology and Geothermal Research*, *326*, 2–25. https://doi.org/10.1016/j.jvolgeores.2016.01.017

Crutzen, P. J. (1976). The possible importance of CSO for the sulfate layer of the stratosphere. *Geophysical Research Letters*, *3*(2), 73–76. https://doi.org/10.1029/gl003i002p00073

Dee, D. P., Uppala, S. M., Simmons, A. J., Berrisford, P., Poli, P., Kobayashi, S., et al. (2011). The ERA-Interim reanalysis: Configuration and performance of the data assimilation system. *Quarterly Journal of the Royal Meteorological Society*, *137*(656), 553–597.

Deshler, T., Johnson, B. J., & Rozier, W. R. (1993). Balloonborne measurements of Pinatubo aerosol during 1991 and 1992 at 41°N: Vertical profiles, size distribution, and volatility. *Geophysical Research Letters*, *20*(14), 1435–1438. https://doi.org/10.1029/93gl01337

Dessler, A. E., Schoeberl, M. R., Wang, T., Davis, S. M., Rosenlof, K. H., & Vernier, J.-P. (2014). Variations of stratospheric water vapor over the past three decades. *Journal of Geophysical Research: Atmospheres*, *119*(22), 12588–12598. https://doi.org/10.1002/2014jd021712

Dhomse, S. S., Emmerson, K. M., Mann, G. W., Bellouin, N., Carslaw, K. S., Chipperfield, M. P., et al. (2014). Aerosol microphysics simulations of the Mt.∼Pinatubo eruption with the UM-UKCA composition-climate model. *Atmospheric Chemistry and Physics*, *14*(20), 11221–11246. https://doi.org/10.5194/acp-14-11221-2014

Dickerson, R. R., Kondragunta, S., Stenchikov, G., Civerolo, K. L., Doddridge, B. G., & Holben, B. N. (1997). The impact of aerosols on solar ultraviolet radiation and photochemical smog. *Science*, *278*(5339), 827–830. https://doi.org/10.1126/science.278.5339.827

Douglass, A. R., Prather, M. J., Hall, T. M., Strahan, S. E., Rasch, P. J., Sparling, L. C., et al. (1999). Choosing meteorological input for the global modeling initiative assessment of high-speed aircraft. *Journal of Geophysical Research*, *104*(D22), 27545–27564. https://doi.org/10.1029/1999jd900827

Ebert, E. E., & Curry, J. A. (1992). A parameterization of ice cloud optical properties for climate models. *Journal of Geophysical Research*, *97*(D4), 3831–3836. https://doi.org/10.1029/91jd02472

English, J. M., Toon, O. B., & Mills, M. J. (2013). Microphysical simulations of large volcanic eruptions: Pinatubo and Toba. *Journal of Geophysical Research: Atmospheres*, *118*(4), 1880–1895. https://doi.org/10.1002/jgrd.50196

Fero, J., Carey, S. N., & Merrill, J. T. (2009). Simulating the dispersal of tephra from the 1991 Pinatubo eruption: Implications for the formation of widespread ash layers. *Journal of Volcanology and Geothermal Research*, *186*(1), 120–131. https://doi.org/10.1016/j.jvolgeores.2009.03.011

Fisher, B. L., Krotkov, N. A., Bhartia, P. K., Li, C., Carn, S. A., Hughes, E., & Leonard, P. J. T. (2019). A new discrete wavelength backscattered ultraviolet algorithm for consistent volcanic SO_2 retrievals from multiple satellite missions. *Atmospheric Measurement Techniques*, *12*(9), 5137–5153. https://doi.org/10.5194/amt-12-5137-2019

Folch, A., Costa, A., & Macedonio, G. (2016). FPLUME-1.0: An integrated volcanic plume model accounting for ash aggregation. *Geoscientific Model Development Discussions*, *8*, 8009–8062. https://doi.org/10.5194/gmdd-8-8009-2015

Fueglistaler, S. (2012). Stepwise changes in stratospheric water vapor?. *Journal of Geophysical Research*, *117*(D13). https://doi.org/10.1029/2012jd017582

Fueglistaler, S., Dessler, A. E., Dunkerton, T. J., Folkins, I., Fu, Q., & Mote, P. W. (2009). Tropical tropopause layer. *Reviews of Geophysics*, *47*(1). https://doi.org/10.1029/2008rg000267

Fueglistaler, S., Liu, Y. S., Flannaghan, T. J., Haynes, P. H., Dee, D. P., Read, W. J., et al. (2013). The relation between atmospheric humidity and temperature trends for stratospheric water. *Journal of Geophysical Research: Atmospheres*, *118*(2), 1052–1074. https://doi.org/10.1002/jgrd.50157

Gao, C., Oman, L., Robock, A., & Stenchikov, G. L. (2007). Atmospheric volcanic loading derived from bipolar ice cores: Accounting for the spatial distribution of volcanic deposition. *Journal of Geophysical Research*, *112*(D9). https://doi.org/10.1029/2006jd007461

Gerstell, M. F., Crisp, J., & Crisp, D. (1995). Radiative forcing of the stratosphere by SO_2 gas, silicate ash, and H_2SO_4 aerosols shortly after the 1982 eruptions of El Chichón. *Journal of Climate*, *8*, 1060–1070. https://doi.org/10.1175/1520-0442(1995)008<1060:rfotsb>2.0.co;2

Ghan, S. J., & Zaveri, R. A. (2007). Parameterization of optical properties for hydrated internally mixed aerosol. *Journal of Geophysical Research*, *112*(D10). https://doi.org/10.1029/2006jd007927

Gómez Martín, J. C., Brooke, J. S. A., Feng, W., Höpfner, M., Mills, M. J., & Plane, J. M. C. (2017). Impacts of meteoric sulfur in the Earth's atmosphere. *Journal of Geophysical Research: Atmospheres*, *122*(14), 7678–7701. https://doi.org/10.1002/2017jd027218

Gouhier, M., Eychenne, J., Azzaoui, N., Guillin, A., Deslandes, M., Poret, M., et al. (2019). Low efficiency of large volcanic eruptions in transporting very fine ash into the atmosphere. *Scientific Reports*, *9*(1), 1449. https://doi.org/10.1038/s41598-019-38595-7

Grell, G. A., & Freitas, S. R. (2014). A scale and aerosol aware stochastic convective parameterization for weather and air quality modeling. *Atmospheric Chemistry and Physics*, *14*(10), 5233–5250. https://doi.org/10.5194/acp-14-5233-2014

Grell, G. A., Peckham, S. E., Schmitz, R., McKeen, S. A., Frost, G., Skamarock, W. C., & Eder, B. (2005). Fully coupled "online" chemistry within the WRF model. *Atmospheric Environment*, *39*(37), 6957–6975. https://doi.org/10.1016/j.atmosenv.2005.04.027

Guo, S., Bluth, G. J. S., Rose, W. I., Watson, I. M., & Prata, A. J. (2004). Re-evaluation of SO_2 release of the 15 June 1991 Pinatubo eruption using ultraviolet and infrared satellite sensors. *Geochemistry, Geophysics, Geosystems*, *5*(4). https://doi.org/10.1029/2003gc000654

Guo, S., Rose, W. I., Bluth, G. J. S., & Watson, I. M. (2004). Particles in the great Pinatubo volcanic cloud of June 1991: The role of ice. *Geochemistry, Geophysics, Geosystems*, *5*(5). https://doi.org/10.1029/2003gc000655

Hamill, P., Jensen, E. J., Russell, P. B., & Bauman, J. J. (1997). The life cycle of stratospheric aerosol particles. *Bulletin of the American Meteorological Society*, *78*(7), 1395–1410. https://doi.org/10.1175/1520-0477(1997)078<1395:TLCOSA>2.0.CO;2

Hansen, J., Lacis, A., Ruedy, R., & Sato, M. (1992). Potential climate impact of Mount Pinatubo eruption. *Geophysical Research Letters*, *19*(2), 215–218. https://doi.org/10.1029/91gl02788

Herzog, M., Graf, H.-F., Textor, C., & Oberhuber, J. M. (1998). The effect of phase changes of water on the development of volcanic plumes. *Journal of Volcanology and Geothermal Research*, *87*(1), 55–74. https://doi.org/10.1016/s0377-0273(98)00100-0

Holasek, R. E., Self, S., & Woods, A. W. (1996). Satellite observations and interpretation of the 1991 Mount Pinatubo eruption plumes. *Journal of Geophysical Research*, *101*(B12), 27635–27655. https://doi.org/10.1029/96jb01179

Holton, J. R., Haynes, P. H., McIntyre, M. E., Douglass, A. R., Rood, R. B., & Pfister, L. (1995). Stratosphere-troposphere exchange. *Reviews of Geophysics*, *33*(4), 403–439. https://doi.org/10.1029/95rg02097

Hong, S.-Y., Dudhia, J., & Chen, S.-H. (2004). A revised approach to ice microphysical processes for the bulk parameterization of clouds and precipitation. *Monthly Weather Review*, *132*(1), 103–120. https://doi.org/10.1175/1520-0493(2004)132<0103:ARATIM>2.0.CO;2

Hu, Z., Zhao, C., Huang, J., Leung, L. R., Qian, Y., Yu, H., et al. (2016). Trans-Pacific transport and evolution of aerosols: Evaluation of quasi-global WRF-Chem simulation with multiple observations. *Geoscientific Model Development*, *9*(5), 1725–1746. https://doi.org/10.5194/gmd-9-1725-2016

Iacono, M. J., Delamere, J. S., Mlawer, E. J., Shephard, M. W., Clough, S. A., & Collins, W. D. (2008). Radiative forcing by long-lived greenhouse gases: Calculations with the AER radiative transfer models. *Journal of Geophysical Research: Atmospheres*, *113*(D13). https://doi.org/10.1029/2008jd009944

Jin, Z., Charlock, T. P., Smith, W. L., Jr, & Rutledge, K. (2004). A parameterization of ocean surface albedo. *Geophysical Research Letters*, *31*(22). https://doi.org/10.1029/2004gl021180

Jones, A. C., Haywood, J. M., Jones, A., & Aquila, V. (2016). Sensitivity of volcanic aerosol dispersion to meteorological conditions: A Pinatubo case study. *Journal of Geophysical Research: Atmospheres*, *121*(12), 6892–6908. https://doi.org/10.1002/2016jd025001

Joshi, M. M., & Shine, K. P. (2003). A GCM study of volcanic eruptions as a cause of increased stratospheric water vapor. *Journal of Climate*, *16*(21), 3525–3534. https://doi.org/10.1175/1520-0442(2003)016<3525:AGSOVE>2.0.CO;2

Junge, C. E., & Manson, J. E. (1961). Stratospheric aerosol studies. *Journal of Geophysical Research*, *66*(7), 2163–2182. https://doi.org/10.1029/jz066i007p02163

Kalenderski, S., & Stenchikov, G. (2016). High-resolution regional modeling of summertime transport and impact of African dust over the Red Sea and Arabian Peninsula. *Journal of Geophysical Research: Atmospheres*, *121*(11), 6435–6458. https://doi.org/10.1002/2015jd024480

Kasten, F. (1968). Falling speed of aerosol particles. *Journal of Applied Meteorology and Climatology*, *7*(5), 944–947. https://doi.org/10.1175/1520-0450(1968)007<0944:FSOAP>2.0.CO;2

Kinne, S., Toon, O. B., & Prather, M. J. (1992). Buffering of stratospheric circulation by changing amounts of tropical ozone a Pinatubo Case Study. *Geophysical Research Letters*, *19*(19), 1927–1930. https://doi.org/10.1029/92gl01937

Kirchner, I., Stenchikov, G. L., Graf, H.-F., Robock, A., & Antuña, J. C. (1999). Climate model simulation of winter warming and summer cooling following the 1991 Mount Pinatubo volcanic eruption. *Journal of Geophysical Research*, *104*(D16), 19039–19055. https://doi.org/10.1029/1999jd900213

Kremser, S., Thomason, L. W., von Hobe, M., Hermann, M., Deshler, T., Timmreck, C., et al. (2016). Stratospheric aerosol-Observations, processes, and impact on climate. *Reviews of Geophysics*, *54*(2), 278–335. https://doi.org/10.1002/2015rg000511

Lary, D. J., Balluch, M., & Bekki, S. (1994). Solar heating rates after a volcanic eruption: The importance of SO_2 absorption. *Quarterly Journal of the Royal Meteorological Society*, *120*(520), 1683–1688. https://doi.org/10.1002/qj.49712052011

LeGrande, A. N., Tsigaridis, K., & Bauer, S. E. (2016). Role of atmospheric chemistry in the climate impacts of stratospheric volcanic injections. *Nature Geoscience*, *9*(9), 652–655. https://doi.org/10.1038/ngeo2771

Long, C. S., & Stowe, L. L. (1994). Using the NOAA/AVHRR to study stratospheric aerosol optical thicknesses following the Mt. Pinatubo Eruption. *Geophysical Research Letters*, *21*(20), 2215–2218. https://doi.org/10.1029/94gl01322

Madronich, S. (1987). Photodissociation in the atmosphere: 1. Actinic flux and the effects of ground reflections and clouds. *Journal of Geophysical Research*, *92*(D8), 9740–9752. https://doi.org/10.1029/jd092id08p09740

Manatt, S. L., & Lane, A. L. (1993). A compilation of the absorption cross-sections of SO_2 from 106 to 403 nm. *Journal of Quantitative Spectroscopy and Radiative Transfer*, *50*(3), 267–276. https://doi.org/10.1016/0022-4073(93)90077-u

Mastin, L. G., Guffanti, M., Servranckx, R., Webley, P., Barsotti, S., Dean, K., et al. (2009). A multidisciplinary effort to assign realistic source parameters to models of volcanic ash-cloud transport and dispersion during eruptions. *Journal of Volcanology and Geothermal Research*, *186*(1), 10–21. https://doi.org/10.1016/j.jvolgeores.2009.01.008

McCormick, M. P., Thomason, L. W., & Trepte, C. R. (1995). Atmospheric effects of the Mt Pinatubo eruption. *Nature*, *373*(6513), 399–404. https://doi.org/10.1038/373399a0

Miguez-Macho, G., Stenchikov, G. L., & Robock, A. (2004). Spectral nudging to eliminate the effects of domain position and geometry in regional climate model simulations. *Journal of Geophysical Research: Atmospheres*, *109*(D13). https://doi.org/10.1029/2003jd004495

Mills, M. J., Schmidt, A., Easter, R., Solomon, S., Kinnison, D. E., Ghan, S. J., et al. (2016). Global volcanic aerosol properties derived from emissions, 1990–2014, using CESM1(WACCM). *Journal of Geophysical Research: Atmospheres*, *121*(5), 2332–2348. https://doi.org/10.1002/2015jd024290

Mlawer, E. J., & Clough, S. A. (1998). Shortwave and longwave enhancements in the rapid radiative transfer model. Paper presented at the *Proceedings of the 7th atmospheric radiation measurement (ARM) Science Team Meeting*. Retrieved from https://www.arm.gov/publications/proceedings/conf07/extended_abs/mlawer_ej.pdf

Mlawer, E. J., Taubman, S. J., Brown, P. D., Iacono, M. J., & Clough, S. A. (1997). Radiative transfer for inhomogeneous atmospheres: RRTM, a validated correlated-k model for the longwave. *Journal of Geophysical Research*, *102*(D14), 16663–16682. https://doi.org/10.1029/97jd00237

Mok, J., Krotkov, N. A., Arola, A., Torres, O., Jethva, H., Andrade, M., et al. (2016). Impacts of brown carbon from biomass burning on surface UV and ozone photochemistry in the Amazon Basin. *Scientific Reports*, *6*(1). 36940. https://doi.org/10.1038/srep36940

Morton, B. R., Taylor, G. I., & Turner, J. S. (1956). Turbulent gravitational convection from maintained and instantaneous sources. *Proceedings of the Royal Society of London—Series A: Mathematical and Physical Sciences*, *234*(1196), 1–23.

Neely, R. R., III, Toon, O. B., Solomon, S., Vernier, J.-P., Alvarez, C., English, J. M., et al. (2013). Recent anthropogenic increases in SO_2 from Asia have minimal impact on stratospheric aerosol. *Geophysical Research Letters*, *40*(5), 999–1004. https://doi.org/10.1002/grl.50263

Niemeier, U., Timmreck, C., Graf, H.-F., Kinne, S., Rast, S., & Self, S. (2009). Initial fate of fine ash and sulfur from large volcanic eruptions. *Atmospheric Chemistry and Physics*, *9*(22), 9043–9057. https://doi.org/10.5194/acp-9-9043-2009

Oman, L., Robock, A., Stenchikov, G. L., Thordarson, T., Koch, D., Shindell, D. T., & Gao, C. (2006). Modeling the distribution of the volcanic aerosol cloud from the 1783–1784 Laki eruption. *Journal of Geophysical Research: Atmospheres*, *111*(D12). https://doi.org/10.1029/2005jd006899

Osipov, S., Stenchikov, G., Brindley, H., & Banks, J. (2015). Diurnal cycle of the dust instantaneous direct radiative forcing over the Arabian Peninsula. *Atmospheric Chemistry and Physics*, *15*(16), 9537–9553. https://doi.org/10.5194/acp-15-9537-2015

Osipov, S., Stenchikov, G., Tsigaridis, K., LeGrande, A. N., & Bauer, S. E. (2020). The role of the SO radiative effect in sustaining the volcanic winter and soothing the Toba impact on climate. *Journal of Geophysical Research: Atmospheres*, *125*(2), e2019JD031726. https://doi.org/10.1029/2019jd031726

Petters, M. D., & Kreidenweis, S. M. (2007). A single parameter representation of hygroscopic growth and cloud condensation nucleus activity. *Atmospheric Chemistry and Physics*, *7*(8), 1961–1971. https://doi.org/10.5194/acp-7-1961-2007

Pinto, J. P., Turco, R. P., & Toon, O. B. (1989). Self-limiting physical and chemical effects in volcanic eruption clouds. *Journal of Geophysical Research*, *94*(D8), 11165–11174. https://doi.org/10.1029/jd094id08p11165

Pollack, J. B., Toon, O. B., & Khare, B. N. (1973). Optical properties of some terrestrial rocks and glasses. *Icarus*, *19*(3), 372–389. https://doi.org/10.1016/0019-1035(73)90115-2

Pollack, J. B., Toon, O. B., Sagan, C., Summers, A., Baldwin, B., & Van Camp, W. (1976). Volcanic explosions and climatic change: A theoretical assessment. *Journal of Geophysical Research*, *81*(6), 1071–1083. https://doi.org/10.1029/jc081i006p01071

Powers, J. G., Klemp, J. B., Skamarock, W. C., Davis, C. A., Dudhia, J., Gill, D. O., et al. (2017). The weather research and forecasting model: Overview, system efforts, and future directions. *Bulletin of the American Meteorological Society*, *98*(8), 1717–1737. https://doi.org/10.1175/BAMS-D-15-00308.1

Pueschel, R. F. (1996). Stratospheric aerosols: Formation, properties, effects. *Journal of Aerosol Science*, *27*(3), 383–402. https://doi.org/10.1016/0021-8502(95)00557-9

Pueschel, R. F., Russell, P. B., Allen, D. A., Ferry, G. V., Snetsinger, K. G., Livingston, J. M., & Verma, S. (1994). Physical and optical properties of the Pinatubo volcanic aerosol: Aircraft observations with impactors and a Sun-tracking photometer. *Journal of Geophysical Research*, *99*(D6), 12915–12922. https://doi.org/10.1029/94jd00621

Ramaswamy, V., Collins, W., Haywood, J., Lean, J., Mahowald, N., Myhre, G., et al. (2019). Radiative forcing of climate: The historical evolution of the radiative forcing concept, the forcing agents and their quantification, and applications. *Meteorological Monographs*, *59*, 1411–14101. https://doi.org/10.1175/amsmonographs-d-19-0001.1

Randel, W. J., Wu, F., Oltmans, S. J., Rosenlof, K., & Nedoluha, G. E. (2004). Interannual changes of stratospheric water vapor and correlations with tropical tropopause temperatures. *Journal of the Atmospheric Sciences*, *61*(17), 2133–2148. https://doi.org/10.1175/1520-0469(2004)061<2133:ICOSWV>2.0.CO;2

Rasch, P. J., Tilmes, S., Turco, R. P., Robock, A., Oman, L., Chen, C.-C., et al. (2008). An overview of geoengineering of climate using stratospheric sulfate aerosols. *Philosophical Transactions of the Royal Society A: Mathematical, Physical and Engineering Sciences*, *366*(1882), 4007–4037. https://doi.org/10.1098/rsta.2008.0131

Read, W. G., Froidevaux, L., & Waters, J. W. (1993). Microwave limb sounder measurement of stratospheric SO_2 from the Mt. Pinatubo Volcano. *Geophysical Research Letters*, *20*(12), 1299–1302. https://doi.org/10.1029/93gl00831

Robock, A. (2000). Volcanic eruptions and climate. *Reviews of Geophysics*, *38*(2), 191–219. https://doi.org/10.1029/1998rg000054

Robock, A., Ammann, C. M., Oman, L., Shindell, D., Levis, S., & Stenchikov, G. (2009). Did the Toba volcanic eruption of ~74 ka B.P. produce widespread glaciation?. *Journal of Geophysical Research*, *114*(D10), D10107. https://doi.org/10.1029/2008JD011652

Rosenlof, K. H. (1995). Seasonal cycle of the residual mean meridional circulation in the stratosphere. *Journal of Geophysical Research*, *100*(D3), 5173–5191. https://doi.org/10.1029/94jd03122

Russell, P. B., Livingston, J. M., Pueschel, R. F., Bauman, J. J., Pollack, J. B., Brooks, S. L., et al. (1996). Global to microscale evolution of the Pinatubo volcanic aerosol derived from diverse measurements and analyses. *Journal of Geophysical Research*, *101*(D13), 18745–18763. https://doi.org/10.1029/96jd01162

Schmidt, A., Mills, M. J., Ghan, S., Gregory, J. M., Allan, R. P., Andrews, T., et al. (2018). Volcanic radiative forcing from 1979 to 2015. *Journal of Geophysical Research - D: Atmospheres*, *123*(22), 12491–12508. https://doi.org/10.1029/2018jd028776

Sekiya, T., Sudo, K., & Nagai, T. (2016). Evolution of stratospheric sulfate aerosol from the 1991 Pinatubo eruption: Roles of aerosol microphysical processes. *Journal of Geophysical Research: Atmospheres*, *121*(6), 2911–2938. https://doi.org/10.1002/2015jd024313

Self, S., Zhao, J.-X., Holasek, R. E., Torres, R. C., & King, A. J. (1996). The atmospheric impact of the Mount Pinatubo eruption. In C. G. Newhall, & R. S. Punongbayan (Eds.), *Fire and mud: Eruptions and lahars of Mount Pinatubo, Philippines* (pp. 1089–1115). Seattle, WA: Philippine Institute of Volcanology and Seismology, Quezon City, and University of Washington Press.

Sheng, J.-X., Weisenstein, D. K., Luo, B.-P., Rozanov, E., Stenke, A., Anet, J., et al. (2015). Global atmospheric sulfur budget under volcanically quiescent conditions: Aerosol-chemistry-climate model predictions and validation. *Journal of Geophysical Research: Atmospheres*, *120*(1), 256–276. https://doi.org/10.1002/2014jd021985

Shepherd, J. (2009). *Geoengineering the climate: Science, governance and uncertainty*. Royal Society. Retrieved from https://royalsociety.org/topics-policy/publications/2009/geoengineering-climate/

Sigl, M., Winstrup, M., McConnell, J. R., Welten, K. C., Plunkett, G., Ludlow, F., et al. (2015). Timing and climate forcing of volcanic eruptions for the past 2,500 years. *Nature*, *523*(7562), 543–549. https://doi.org/10.1038/nature14565

Skamarock, W. C., Klemp, J. B., Dudhia, J., Gill, D. O., Barker, D. M., Wang, W., & Powers, J. G. (2005). *A description of the advanced research WRF version 2—Technical Report*. University Corporation for Atmospheric Research. https://doi.org/10.5065/D6DZ069T

Stenchikov, G. (2016). The role of volcanic activity in climate and global change. In T. M. Letcher (Ed.), *Climate change, observed impact on planet Earth* (2nd ed., pp. 419–447). Boston, MA: Elsevier. https://doi.org/10.1016/b978-0-444-63524-2.00026-9

Stenchikov, G. L., Kirchner, I., Robock, A., Graf, H.-F., Antuña, J. C., Grainger, R. G., et al. (1998). Radiative forcing from the 1991 Mount Pinatubo volcanic eruption. *Journal of Geophysical Research*, *103*(D12), 13837–13857. https://doi.org/10.1029/98jd00693

Stenchikov, G. L., Robock, A., Ramaswamy, V., Schwarzkopf, M. D., Hamilton, K., & Ramachandran, S. (2002). Arctic oscillation response to the 1991 Mount Pinatubo eruption: Effects of volcanic aerosols and ozone depletion. *Journal of Geophysical Research: Atmospheres*, *107*(D24). ACL21–ACL16. https://doi.org/10.1029/2002jd002090

Stockwell, W. R., Kirchner, F., Kuhn, M., & Seefeld, S. (1997). A new mechanism for regional atmospheric chemistry modeling. *Journal of Geophysical Research*, *102*(D22), 25847–25879. https://doi.org/10.1029/97jd00849

Strahan, S. E., Douglass, A. R., Stolarski, R. S., Akiyoshi, H., Bekki, S., Braesicke, P., et al. (2011). Using transport diagnostics to understand chemistry climate model ozone simulations. *Journal of Geophysical Research: Atmospheres*, *116*(D17). https://doi.org/10.1029/2010jd015360

Suzuki, Y. J., Costa, A., Cerminara, M., Esposti Ongaro, T., Herzog, M., Van Eaton, A. R., & Denby, L. C. (2016). Inter-comparison of three-dimensional models of volcanic plumes. *Journal of Volcanology and Geothermal Research*, *326*, 26–42. https://doi.org/10.1016/j.jvolgeores.2016.06.011

Textor, C., Graf, H.-F., Herzog, M., & Oberhuber, J. M. (2003). Injection of gases into the stratosphere by explosive volcanic eruptions. *Journal of Geophysical Research*, *108*(D19). https://doi.org/10.1029/2002jd002987

Textor, C., Graf, H.-F., Timmreck, C., & Robock, A. (2004). Emissions from volcanoes. In *Advances in global change research* (Vol. 18). https://doi.org/10.1038/sj.jhh.1001766

Thomason, L. W. (1992). Observations of a new SAGE II aerosol extinction mode following the eruption of Mt. Pinatubo. *Geophysical Research Letters*, *19*(21), 2179–2182. https://doi.org/10.1029/92gl02185

Thomason, L. W., Ernest, N., Millán, L., Rieger, L., Bourassa, A., Vernier, J.-P., et al. (2018). A global space-based stratospheric aerosol climatology: 1979-2016. *Earth System Science Data*, *10*(1), 469–492. https://doi.org/10.5194/essd-10-469-2018

Thomason, L. W., & Peter, T. (2006). *Assessment of stratospheric aerosol properties* (WCRP-124, WMO/TD-1295, SPARC Report 4). Retrieved from https://www.sparc-climate.org/data-centre/data-access/assessment-of-stratospheric-aerosol-properties/

Tie, X., Brasseur, G. P., Briegleb, B., & Granier, C. (1994). Two-dimensional simulation of Pinatubo aerosol and its effect on stratospheric ozone. *Journal of Geophysical Research*, *99*(D10), 20545–20562. https://doi.org/10.1029/94jd01488

Timmreck, C. (2012). Modeling the climatic effects of large explosive volcanic eruptions. *WIREs Climate Change*, *3*(6), 545–564. https://doi.org/10.1002/wcc.192

Timmreck, C., Graf, H.-F., & Kirchner, I. (1999). A one and half year interactive MA/ECHAM4 simulation of Mount Pinatubo Aerosol. *Journal of Geophysical Research*, *104*(D8), 9337–9359. https://doi.org/10.1029/1999JD900088

Timmreck, C., Graf, H.-F., Lorenz, S. J., Niemeier, U., Zanchettin, D., Matei, D., et al. (2010). Aerosol size confines climate response to volcanic super-eruptions. *Geophysical Research Letters*, *37*(24). https://doi.org/10.1029/2010gl045464

Timmreck, C., Mann, G. W., Aquila, V., Hommel, R., Lee, L. A., Schmidt, A., et al. (2018). The interactive stratospheric aerosol model intercomparison project (ISA-MIP): Motivation and experimental design. *Geoscientific Model Development*, *11*(7), 2581–2608. https://doi.org/10.5194/gmd-11-2581-2018

Trepte, C. R., & Hitchman, M. H. (1992). Tropical stratospheric circulation deduced from satellite aerosol data. *Nature*, *355*(6361), 626–628. https://doi.org/10.1038/355626a0

Turco, R. P., Whitten, R. C., & Toon, O. B. (1982). Stratospheric aerosols: Observation and theory. *Reviews of Geophysics*, *20*(2), 233–279. https://doi.org/10.1029/rg020i002p00233

Ukhov, A., Ahmadov, R., Grell, G., & Stenchikov, G. (2021). Improving dust simulations in WRF-Chem v4.1.3 coupled with the GOCART aerosol module. *Geoscientific Model Development*, *14*, 473–493. https://doi.org/10.5194/gmd-14-473-2021

Ukhov, A., Mostamandi, S., da Silva, A., Flemming, J., Alshehri, Y., Shevchenko, I., & Stenchikov, G. (2020). Assessment of natural and anthropogenic aerosol air pollution in the Middle East using MERRA-2, CAMS data assimilation products, and high-resolution WRF-Chem model simulations. *Atmospheric Chemistry and Physics*, *20*, 1–42

Ukhov, A., Mostamandi, S., Krotkov, N., Flemming, J., da Silva, A., Li, C., et al. (2020). Study of SO pollution in the Middle East using MERRA-2, CAMS data assimilation products, and high-resolution WRF-Chem Simulations. *Journal of Geophysical Research: Atmospheres*, *125*(6). e2019JD031993. https://doi.org/10.1029/2019jd031993

Vernier, J.-P., Fairlie, T. D., Deshler, T., Natarajan, M., Knepp, T., Foster, K., et al. (2016). In situ and space-based observations of the Kelud volcanic plume: The persistence of ash in the lower stratosphere. *Journal of Geophysical Research: Atmospheres*, *121*(18), 11104–11118. https://doi.org/10.1002/2016jd025344

Vernier, J.-P., Thomason, L. W., Pommereau, J.-P., Bourassa, A., Pelon, J., Garnier, A., et al. (2011). Major influence of tropical volcanic eruptions on the stratospheric aerosol layer during the last decade. *Geophysical Research Letters*, *38*(12). https://doi.org/10.1029/2011gl047563

Vogel, A., Diplas, S., Durant, A. J., Azar, A. S., Sunding, M. F., Rose, W. I., et al. (2017). Reference data set of volcanic ash physicochemical and optical properties. *Journal of Geophysical Research: Atmospheres*, *122*(17), 9485–9514. https://doi.org/10.1002/2016jd026328

Vogel, H., Förstner, J., Vogel, B., Hanisch, T., Mühr, B., Schättler, U., & Schad, T. (2014). Time-lagged ensemble simulations of the dispersion of the Eyjafjallajökull plume over Europe with COSMO-ART. *Atmospheric Chemistry and Physics*, *14*(15), 7837–7845. https://doi.org/10.5194/acp-14-7837-2014

Weisenstein, D. K., Yue, G. K., Ko, M. K. W., Sze, N.-D., Rodriguez, J. M., & Scott, C. J. (1997). A two-dimensional model of sulfur species and aerosols. *Journal of Geophysical Research*, *102*(D11), 13019–13035. https://doi.org/10.1029/97jd00901

Wiesner, M. G., Wetzel, A., Catane, S. G., Listanco, E. L., & Mirabueno, H. T. (2004). Grain size, areal thickness distribution and controls on sedimentation of the 1991 Mount Pinatubo tephra layer in the South China Sea. *Bulletin of Volcanology*, *66*(3), 226–242. https://doi.org/10.1007/s00445-003-0306-x

Winker, D. M., & Osborn, M. T. (1992). Airborne lidar observations of the Pinatubo volcanic plume. *Geophysical Research Letters*, *19*(2), 167–170. https://doi.org/10.1029/91gl02867

Woods, A. W. (2010). Turbulent plumes in nature. *Annual Review of Fluid Mechanics*, *42*(1), 391–412. https://doi.org/10.1146/annurev-fluid-121108-145430

Young, R. E., Houben, H., & Toon, O. B. (1994). Radiatively forced dispersion of the Mt. Pinatubo volcanic cloud and induced temperature perturbations in the stratosphere during the first few months following the eruption. *Geophysical Research Letters*, *21*(5), 369–372. https://doi.org/10.1029/93gl03302

Zhao, J., Turco, R. P., & Toon, O. B. (1995). A model simulation of Pinatubo volcanic aerosols in the stratosphere. *Journal of Geophysical Research*, *100*(D4), 7315–7328. https://doi.org/10.1029/94jd03325

Zhong, W., Haigh, J. D., Toumi, R., & Bekki, S. (1996). Infrared heating rates in the stratosphere due to volcanic sulphur dioxide. *Quarterly Journal of the Royal Meteorological Society*, *122*(534), 1459–1466. https://doi.org/10.1002/qj.49712253411

Zhu, Y., Toon, O. B., Jensen, E. J., Bardeen, C. G., Mills, M. J., Tolbert, M. A., et al. (2020). Persisting volcanic ash particles impact stratospheric SO_2 lifetime and aerosol optical properties. *Nature Communications*, *11*(1), 4526. https://doi.org/10.1038/s41467-020-18352-5